

## Spherical Nucleic Acids

Joshua I. Cutler, Evelyn Auyeung, and Chad A. Mirkin\*

Department of Chemistry and International Institute for Nanotechnology, Northwestern University, 2145 Sheridan Road, Evanston, Illinois 60208, United States

### Supporting Information

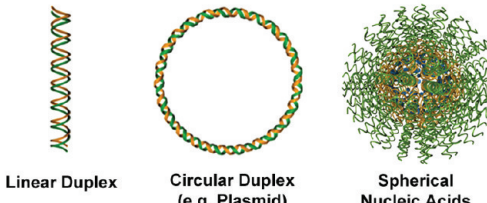
**ABSTRACT:** A historical perspective of the development of spherical nucleic acid (SNA) conjugates and other three-dimensional nucleic acid nanostructures is provided. This Perspective details the synthetic methods for preparing them, followed by a discussion of their unique properties and theoretical and experimental models for understanding them. Important examples of technological advances made possible by their fundamental properties spanning the fields of chemistry, molecular diagnostics, gene regulation, medicine, and materials science are also presented.

### 1. INTRODUCTION

In 1996, we introduced a synthetic method for preparing polyvalent nucleic acid–nanoparticle conjugates, spherical nanostructures with densely functionalized and highly oriented nucleic acids covalently attached to their surfaces (Figure 1).<sup>1</sup> These structures represent the first well-characterized forms of spherical nucleic acid (SNA) conjugates and were originally made with gold cores and DNA shells.<sup>1</sup> Moreover, they exhibit properties that are distinct from those of both the nanoparticles (NPs) and DNA from which they derive. Since the initial work, these materials have been used in many important, and in certain cases, commercially viable applications; indeed, they have catalyzed worldwide interest in using well-characterized nanostructures as novel labels for *in vitro* biodetection schemes<sup>2–7</sup> and intracellular assays,<sup>8–11</sup> and as potent cell transfection,<sup>12–15</sup> therapeutic,<sup>16</sup> and gene regulation materials.<sup>15,17–19</sup> Subsequent studies have shown that the inorganic NPs serve two purposes: (1) they provide novel physical and chemical properties (e.g., plasmonic, catalytic, scattering, quenching) that are especially important in the contexts of materials design and nanoparticle probe design, and (2) they act as a scaffold for assembling and orienting the oligonucleotides into a dense arrangement that gives rise to many of their functional properties. Significantly, recent studies have shown that one can use the gold core as a scaffold, subsequently cross-link the DNA at the base of the particle, and dissolve the gold to create a new coreless form of SNAs, exhibiting many of the hallmark properties of the original gold nanoparticle (Au NP) conjugates, including the ability to cooperatively hybridize complementary nucleic acids and efficiently transfect cell membranes without the need for co-carriers.<sup>20</sup> This work underscored one of the fundamental features of SNAs, namely, that many of the properties of these nanostructures stem from a dense layer of oriented nucleic acids and are core-independent.

This Perspective aims to provide a historical overview of the development of such SNA conjugates by first exploring

### A Structural Forms of Nucleic Acids



### B Modes of Assembly

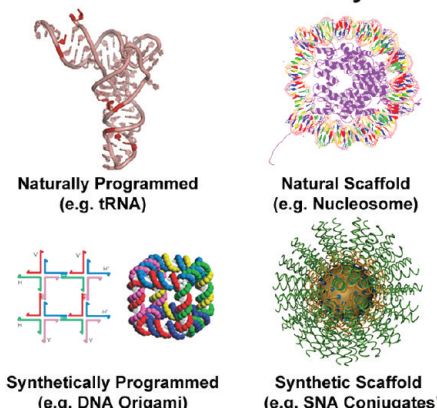


**Figure 1.** (A) Existing structural forms of nucleic acids include linear duplexes, circular plasmid DNA, and three-dimensional SNA. (B) Nucleic acid structures with well-defined shapes are made naturally through sequence selection and base-pairing interactions or through synthetic means (left). Alternatively, templates such as proteins or synthetic nanostructures can be used to make highly functional architectures based upon the size and shape of the template (right). Figures are not drawn to scale. Transfer RNA image adapted with permission from ref 33. Copyright 2011 Nature Publishing Group. Nucleosome core adapted with permission from ref 32. Copyright 1997 Nature Publishing Group. DNA origami image adapted with permission from ref 36. Copyright 2003 Nature Publishing Group.

synthetic methods for preparing them, followed by a discussion of their unique properties and a basis for understanding them. We will then highlight important examples of technological advances made possible by their fundamental properties spanning the fields of chemistry, biology, medicine, and materials science. As there is still much to be learned from the use of these materials, an important goal of this Perspective is to inspire future investigations of spherical and other three-dimensional (3D) nucleic acid-based structures.

Received: October 4, 2011

Published: January 9, 2012



## 2. THE EMERGENCE OF DNA AS A SURFACE LIGAND FOR NANOPARTICLES

The ligands attached to a NP's surface (the ligand shell) are responsible for governing much of a NP's overall chemistry and its stability in complex media. These molecules are typically designed with a headgroup moiety suitable for attachment to the NP of interest and a tail group that extends into the solution, helps maintain colloidal stability, and controls particle reactivity. In the 1990s, the synthesis of chemically well-defined nanocrystals with well-characterized ligand shells<sup>21,22</sup> became a major focus, with one of the intended uses of such structures being to prepare colloidal assemblies or superstructures.<sup>23</sup> Much of the work focused on using simple hydrocarbon surfactant ligands such as negatively charged carboxylates<sup>24</sup> or positively charged ammonium functional groups<sup>25</sup> that could influence the charge and solubility of the particles. However, if the intent is to use such particle building blocks to make superstructures and colloidal crystals, control over the architectural parameters of the resulting assemblies and materials is quite limited with conventional small-molecule adsorbates. Therefore, in 1996, we reported a novel strategy for preparing water-soluble conjugates from aqueous citrate-stabilized Au NPs and alkylthiol-functionalized DNA.<sup>1</sup> This approach, at the time, represented a departure from the concurrent and extensive efforts to characterize well-formed alkanethiol monolayers on gold surfaces,<sup>26,27</sup> but it was a natural extension of our work that focused on making redox-active monolayers from ferrocenyl- and alkanethiol-capped oligonucleotides on bulk gold electrode surfaces.<sup>28</sup>

The structures synthesized in the original work consisted of 13 nm gold cores densely functionalized with a surface shell of DNA coordinated via sulfur groups to the gold; they were the first well-characterized SNA–NP conjugates. Concurrently, Alivisatos and co-workers were developing techniques to prepare monovalent forms of smaller particles (2 nm) with the idea of using DNA templates to arrange individual particles in a controllable manner on such templates.<sup>29</sup> These structures have led to interesting advances in their own right, including the development of the concept of a plasmon ruler,<sup>30,31</sup> but they do not possess the structure and properties of the SNA conjugate analogues, which are the focus of this Perspective. Furthermore, it is important to differentiate the structure of SNA from other forms of nucleic acids (Figure 1).<sup>32–35</sup> The primary difference between SNAs and linear nucleic acids is that SNAs are dense, oriented spherical arrays of short oligonucleotides. While most forms of nucleic acids rely on the hybridized duplex as the fundamental structural unit that determines their overall shape, SNAs can be prepared from both single- and double-stranded nucleic acids, and their orientation is determined by the shape of the inorganic core. SNA nanostructures are also distinct from the synthetic structures made in the field, often referred to as "DNA nanotechnology and origami", wherein the recognition properties of DNA are used to assemble duplexes into rationally designed shapes.<sup>36–38</sup> The physical SNA structures described herein are synthesized independent of nucleic acid sequence and hybridization; they are formed via chemical bonds, not recognition processes.

## 3. STRUCTURAL CONSIDERATIONS FOR SNA AND SNA–NP CONJUGATES

SNA nanostructures are chemically quite sophisticated and can have markedly different properties depending upon the components and their placement within such structures (Figure 2). For example, they have higher binding constants for their

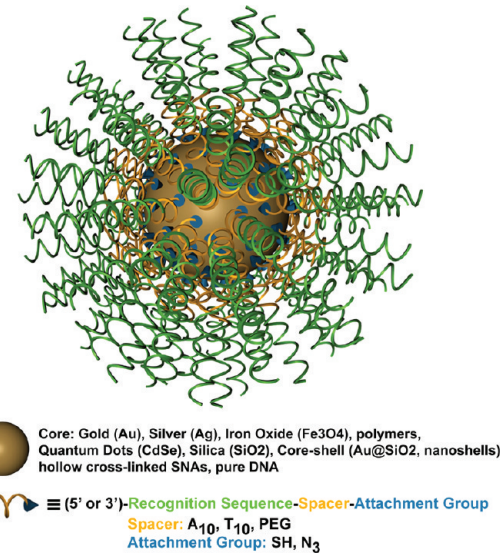


**Figure 2.** The anatomy of SNA nanostructures. An inorganic core is densely functionalized with oligonucleotides containing three segments: a recognition sequence, a spacer segment, and a chemical-attachment group. Additionally, other functional groups such as dye molecules, quenchers, modified bases, and drugs can be attached along any segment of the oligonucleotide.

complements than free strands of the same sequence,<sup>39</sup> exhibit cooperative binding and subsequent sharp melting transitions,<sup>1,40</sup> are resistant to nuclease degradation,<sup>41</sup> and are capable of transfecting cell lines without the need for ancillary physical or chemical transfection methods.<sup>15</sup> Although these materials often contain an inorganic core, the emergent properties unique to SNAs stem in large part from the density and orientation of the oligonucleotides at the outer region of the nanostructure (section 5). However, structures with cores (e.g., Au,<sup>1</sup> Ag,<sup>42</sup> Fe<sub>3</sub>O<sub>4</sub>,<sup>43</sup> CdSe,<sup>44</sup> nanoshells,<sup>23</sup> core shell structures,<sup>45,46</sup> and polymers<sup>47,48</sup>) can confer additional properties to the conjugate, which derive from the physical and chemical characteristics of the nanostructured core materials.<sup>49</sup> Finally, designer nucleic acids<sup>50</sup> can provide additional functionality, all of which can be exploited in the design of molecular diagnostic systems<sup>11</sup> and gene regulating structures,<sup>51,52</sup> and in materials synthesis.<sup>20</sup> Below, we outline some of the general design considerations of SNA–NPs, their unusual properties, and what is understood about the structure–function relationships of these materials.

An initial design consideration for SNA conjugates is the core material. The properties of the oligonucleotide shell are now well-studied and highly predictable based on its structure; an additional way to tailor the behavior of SNA conjugates is through the choice of the core material. Thus far, the most widely studied conjugates have consisted of Au NP cores functionalized with alkylthiolated oligonucleotides attached through an Au–S bond at the 3' or 5' end of the molecule.<sup>1,53,54</sup> Au NPs were chosen as initial candidates for the core material because they are easily synthesized over a range of particle diameters,<sup>55</sup> have plasmon resonances with high extinction coefficients, can be easily functionalized with a wide variety of chemical reagents, and exhibit well-defined catalytic properties. When modified with a dense monolayer of DNA, these particles, in addition to all SNAs, exhibit properties that are extremely useful in molecular diagnostic,<sup>5</sup> therapeutic,<sup>15</sup> and materials applications (Table 1).<sup>56,57</sup> In addition to gold, the physical properties of other inorganic NPs offer unique benefits within the SNA paradigm. To that end, there has been a

Table 1

property	spherical nucleic acids	linear nucleic acids
melting transition	cooperative and narrow ( $\sim 2\text{--}8^\circ\text{C}$ )	broad ( $\sim 20^\circ\text{C}$ )
cellular uptake	transfection agents <i>not</i> required, $(1\text{--}1.5) \times 10^6$ NPs per cell <sup>a</sup>	transfection agents required (e.g., DharmaFECT, Lipofectamine, $\text{Ca}^{2+}$ )
immune response	minimal <sup>141</sup>	elevated interferon- $\beta$ levels (25-fold increase compared to DNA–Au NP conjugates) <sup>141</sup>
stability	nuclease resistance due to high local salt concentration <sup>41</sup>	subject to degradation by nucleases (e.g., DNase degradation 4 $\times$ higher rate than SNA)
properties from inorganic core	plasmonic, catalytic, <sup>5,20</sup> magnetic, <sup>43</sup> luminescent <sup>44</sup>	n/a
binding strength <sup>b</sup>	$K_{\text{eq}} = 1.8 \times 10^{14}$ , activated binding motifs <sup>150</sup>	$K_{\text{eq}} = 1.8 \times 10^{12}$

<sup>a</sup>Numbers vary depending on cell type and nucleic acid sequence. <sup>b</sup> $K_{\text{eq}}$  values for 15-mer AT-rich strand.<sup>39</sup>

significant effort to attach oligonucleotides to a wide range of particle types, including silver,<sup>42</sup> semiconductor quantum dots (QDs),<sup>44</sup> silica,<sup>58</sup> and metal oxides<sup>43</sup> to form SNA architectures. It is important to note that each of these methods requires specific chemistry tailored to the particles of interest, which is a nontrivial task due to the oligonucleotide densities necessary to achieve the properties unique to SNAs (section 4). For example, the surfaces of aqueous silver nanoparticles (Ag NPs) are easily oxidized,<sup>59,60</sup> which makes it difficult to prepare stable conjugates from monodentate alkylthiols. Therefore, SNAs from Ag NPs are typically prepared from oligonucleotides with multiple cyclic disulfide anchoring groups.<sup>42</sup> Alternatively, silver nanoprisms have been functionalized with DNA by first coating them with a silica shell with subsequent bioconjugation.<sup>58</sup> Cadmium selenide (CdSe) QDs have been functionalized via a three-step processes that entails ligand exchange, solvent exchange, and incubation with alkylthiol-functionalized oligonucleotides.<sup>44</sup> Another method to prepare CdSe/ZnS QDs utilized a novel peptidic linker as an attachment group.<sup>61</sup> Superparamagnetic iron oxide nanoaparticles (SPIONs) have been modified with a SNA shell by using copper-catalyzed alkyne–azide “click” chemistry.<sup>43</sup> Importantly, the DNA binding behavior of these conjugates, which stems from their dense oligonucleotide monolayer, is nearly identical regardless of core material (*vide infra*, Table 1).

The oligonucleotides comprising SNAs consist of three main components: a particle attachment moiety (in the case of particle based structures), a spacer region, and a programmable recognition region. Each group serves an integral role for the function of the SNA, and each unit has been the subject of multiple studies. For Au NPs, a typical attachment group is a single propyl- or hexylthiol group, which can be incorporated through traditional phosphoramidite chemistry (usually at the 5' or 3' ends, but in principle can be incorporated anywhere along the sequence). The lack of side reactions for the adsorption of thiols on gold allows for the functionalization reaction to proceed for as long as desired, and yields very high oligonucleotide densities on the surfaces of the Au NPs. Other attachment groups have been used to obtain conjugates with higher stabilities, such as those with chelating moieties, e.g., cyclic disulfides<sup>62,63</sup> or branched thiol structures.<sup>53</sup> A typical test of conjugate stability involves an evaluation of the rate of oligonucleotide displacement with the disulfide reducing agent dithiothreitol.<sup>62</sup> The second segment of the oligonucleotide sequence, the spacer group, pushes the recognition region away from the Au NP surface, and can be composed of DNA bases (e.g., T<sub>10</sub> or A<sub>10</sub>) or other synthetic groups such as polyethylene

glycol (PEG) units.<sup>64</sup> Finally, the recognition portion of the strand is tailored for each investigation or technological use and is generally the active segment that is available for further base-pairing with other strands of interest (e.g., linker strands with sticky ends, target strands in detection assays, or complementary strands for the formation of siRNA). This portion can be composed of any such unit that can be incorporated via phosphoramidite chemistry, which in the simplest form is based on conventional nucleic acids (DNA or RNA).

In addition to DNA or RNA, the modularity afforded by phosphoramidite chemistry allows for incorporation of a wide variety of modifications to the nucleic acid strands within the SNA architecture. Locked nucleic acid (LNA) bases have been used to increase the binding strength of conjugates to their targets, which, in certain cases, can create a more potent construct.<sup>52</sup> In one example, by incorporating only four LNA bases into the particle sequence, the gene knockdown in A549 lung carcinoma cells by conjugates targeting the survivin gene was improved by 66.6%.<sup>52</sup> McKenzie et al. have shown that LNA–Au NP conjugates can be used to increase the melting temperature of such conjugates by  $\sim 3^\circ\text{C}$  per LNA base (in a 14 bp sequence).<sup>65</sup> This additional stability allows for higher selectivity in detection schemes. Peptide nucleic acids also have been used to prepare stable conjugates that have unusual properties because of the lack of negative charge on the peptide backbone.<sup>66</sup>

Beyond substitutions of the oligonucleotide backbone, bases can be modified and sequences terminated with groups that provide additional functionality. For example, fluorescent tags, such as fluorescein or cyanine dyes, allow for quantification of the average number of strands per particle,<sup>64</sup> and can be used as intracellular spectroscopic handles for the particles or as “flares”<sup>11</sup> in intracellular detection schemes (section 10). Metal complexes, such as *cis*-diamminedichloroplatinum(II) analogues<sup>67</sup> or gadolinium chelates,<sup>68</sup> have been coupled to conjugates to create potent drug delivery vehicles and magnetic resonance imaging contrast agents, respectively. Chemical tags such as alkynes and azides have been used to prepare probes that enable copper ion detection for environmental monitoring purposes.<sup>69</sup> Antibodies have been co-adsorbed with the oligonucleotides on the surface of the particle to create multifunctional probes that have been used in protein detection assays.<sup>70,71</sup> The high stability of the nucleic acid-modified nanostructures in aqueous media can be used to solubilize drugs that are inherently difficult to transfect, such as paclitaxel,<sup>72</sup> in aqueous media through attachment to the conjugate. Indeed, these are chemically versatile structures that allow one to prepare multifunctional materials using the SNA platform.

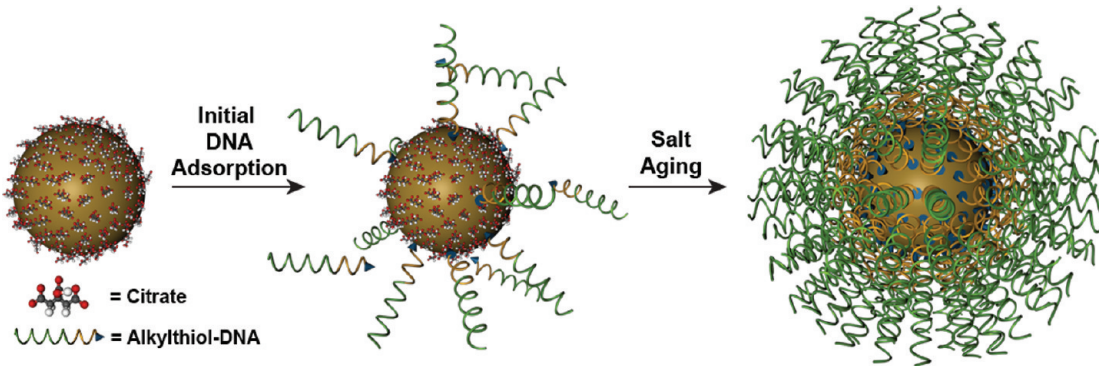


**Figure 3.** Synthesis of SNA–Au NP conjugates. Citrate-stabilized particles are incubated with alkylthiol-functionalized oligonucleotides in water to form a low-density monolayer. By incubating the nanoparticles in aqueous solutions with successively higher concentrations of salt (typically 0.15–1.0 M) and surfactants over ~12 h, a high-density SNA shell is formed.

#### 4. CONTROLLING THE DENSITY OF SNA CONJUGATES

Initial studies conducted with DNA–Au NPs have demonstrated the potential for utilizing SNA conjugates across a large number of disciplines. Indeed, the first reports of these structures touched off a decade and a half of research that continues today, which branched from materials synthesis to fundamental studies in DNA–NP-based assembly, diagnostics, and therapeutics (sections 6, 8, and 9, respectively). The extension of these conjugates to such fields was predicated on their high stability and unique function, which is directly dependent on the structure and density of the monolayer of oligonucleotides on the surface of the NPs. Therefore, it was necessary to understand the important synthetic parameters for producing relatively well-defined conjugates exhibiting properties that have been optimized for an intended use. To that end, the variables that control the loading of oligonucleotides have been studied in detail. These include the salt concentration of the reaction solution, the size and shape of the NP, the bases closest to the particle surface, sonication or heating, and the identity of the chemical attachment moiety.

The first generation of SNA–NP conjugates consisted of citrate-stabilized 13 nm Au NPs that were functionalized with relatively short oligonucleotides through a terminal alkylthiol (e.g., 3'-propylthiol-TACCGTTG).<sup>1</sup> However, because DNA is negatively charged and cannot pack densely without electrostatic screening, only a low-density monolayer was formed, and the resulting particles were only stable on the order of weeks. In a report published soon thereafter,<sup>73</sup> we developed a method to prepare robust conjugates that introduced the concept of salt-aging, which allows for high-density packing of oligonucleotides on the NP's surface, and is now the preferred method for synthesizing such conjugates (Figure 3). Increasing the sodium ion concentration of the reaction solution to >0.15 M (up to ~2.0 M with surfactants) screens the repulsive interactions between neighboring strands, thereby promoting higher densities as the oligonucleotides assemble on the surface of the Au NPs; higher salt concentrations generally result in higher oligonucleotide densities until steric constraints prohibit further adsorption. The monolayer of oligonucleotides formed by this method is especially stable because of the relatively strong Au–S interaction (compared to the Au–citrate interaction). Furthermore, the combined negative charge of the oligonucleotides on the surface of the NPs confers a high negative zeta potential (<−30 mV) that helps stabilize the

colloid from flocculation.<sup>21,74</sup> Indeed, particles functionalized in this way exhibit long-term (months) stability in solutions over a wide range of pH, solvent, and ionic strength conditions. Although DNA disassociation has been observed in certain cases,<sup>25</sup> at room temperature or physiological conditions, we have not observed evidence of significant dissociation.<sup>15</sup> This stability is important for their use in intracellular gene regulation, *in vitro* molecular diagnostic, and materials assembly applications.

The maximum possible surface density of DNA is dependent on the particle size and shape. In the case of spherical particles, smaller particles can support higher densities, substantially greater than values obtained on planar surfaces. For example, 10 nm particles can typically support  $\sim 2.0 \times 10^{13}$  oligos/cm<sup>2</sup>, while the surface coverage for oligonucleotides of the same sequence assembled under identical conditions on a macroscopic planar gold surface is  $5.8 \times 10^{12}$  oligos/cm<sup>2</sup>.<sup>75</sup> In general, a smaller particle can support a higher oligonucleotide density than larger particles because the radius of curvature is higher, which confers a natural deflection angle between neighboring strands that creates additional space around individual strands (Figure 4A). This effect diminishes as the particles increase in

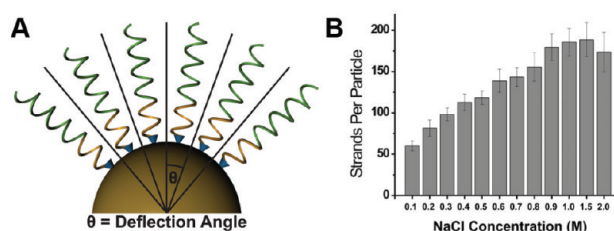


**Figure 4.** (A) The oligonucleotides that comprise SNAs are arranged in a dense, oriented fashion. On a nanoparticle surface, the geometric configuration confers a natural deflection angle between strands. On smaller particles, this angle is greater due to their higher relative curvatures. Ultimately, this results in reduced Coulombic repulsion at the termini of the strands, and hence higher densities in the overall structure. (B) The density of oligonucleotides of SNA–Au NP conjugates is controlled in part by the salt concentration of the NP/DNA incubation solution. A higher salt concentration results in a higher oligonucleotide density. For 15 nm particles, this range spans ~50–200 strands/particle. Reproduced with permission from ref 75. Copyright 2009 American Chemical Society.

size; in fact, at diameters of 200 nm or larger, the surface coverage of DNA approaches that of planar gold.<sup>75</sup> The high-curvature particles result in surfaces with greater free volume

and therefore minimized steric and electronic repulsion constraints, allowing for higher DNA surface densities. By increasing the salt concentration in the reaction solution, this screening is increased, allowing for a greater number of strands per particle (Figure 4B). Finally, a geometric model developed by Hill et al. demonstrated that by combining the experimental density values for curved and flat surfaces, one could accurately predict the natural loading for anisotropic particles, such as gold nanorods and triangular prisms.<sup>75</sup>

Another variable that controls the loading of oligonucleotides on Au NPs is the composition of the DNA bases closest to the particle surface.<sup>64</sup> In general, a spacer region of approximately 10 nucleotides ( $\sim 3$  nm) is often used to extend the active recognition portion of the oligonucleotide sequence away from the positively charged gold surface. This imparts flexibility that is important for binding and which also lowers steric barriers for accessing the full oligonucleotide sequence in the context of hybridization. DNA bases interact with gold surfaces to varying degrees,<sup>76</sup> depending on the base (e.g., affinity of adenine > affinity of thymine), so the choice of bases used in the spacer region is important. Indeed, for 15 nm Au NPs, the density of oligonucleotides is highest when a T<sub>10</sub> spacer is used (38 pmol/cm<sup>2</sup> for thymine compared to 19 pmol/cm<sup>2</sup> for adenine). Furthermore, higher densities can be obtained if PEG units, which minimally interact with the gold surface, are used as spacers (56 pmol/cm<sup>2</sup>).<sup>64</sup> Another method that has been used to increase the surface density of oligonucleotides is sonication,<sup>64</sup> which allows one to facilitate the kinetics of immobilization, orientation, and packing of the oligonucleotides on the surface of the particle. Alternatively, one can get higher loadings and increased adsorption rates at elevated temperatures.<sup>64</sup>

## 5. COOPERATIVE BINDING WITH HIGH-DENSITY SNA CONJUGATES

SNAs are entities with highly tailorable recognition properties by virtue of nucleic acid sequence. Direct particle–particle hybridization is possible,<sup>42,43</sup> in addition to assembly via linker strands,<sup>1</sup> which occurs through the recognition region of the DNA sequences. One can think of the SNA–NP conjugates as individual building blocks, each with a unique identity dictated by their sequence. The NPs can be brought together through particle–DNA and linker design, which results in a polymeric macroscopic assembly. Because the particles are held together through DNA linkages and their cores do not interact or fuse, the DNA–NP conjugates can be released from the aggregate through dehybridization of the duplexes via heating or by lowering the solution salt concentration. DNA duplexes follow predictable “melting” dehybridization when the temperature is raised above the melting point ( $T_m$ ). The same holds true for SNA conjugates; however, their polyvalent binding behavior differs greatly from that of linear duplexes.<sup>40</sup>

During the early studies of the chemical and physical properties of SNA–Au NP conjugates, a striking observation was made concerning the dehybridization of the aggregates (Figure 5A,B). Typically, dehybridization or “melting” of oligonucleotides occurs over a broad temperature range ( $\sim 20$  °C); however, when the duplex-assembled SNA–Au NPs are heated, this melting transition occurs over a very narrow temperature range ( $\sim 2$ –8 °C) and at a temperature higher than the  $T_m$  of the particle-free DNA duplex (at substantially lower concentrations, Figure 5C). These sharp transitions were also observed for single layers of particles that were hybridized

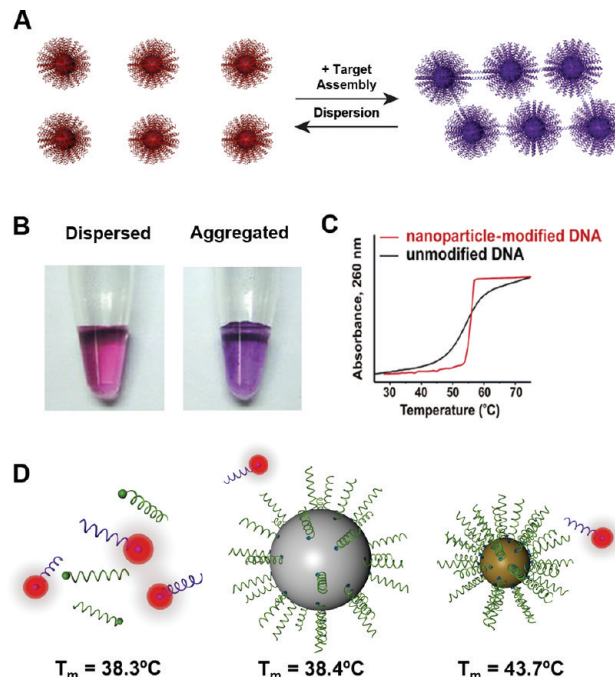


**Figure 5.** (A) Schematic illustration of the aggregation and dispersion of SNA–Au NP conjugates and the corresponding SPR shift of the Au cores. Dispersed particles are red, whereas aggregated particles are purple. Targets can be DNA, metal ions, or any molecule that the SNA shell has been programmed to recognize and bind. (B) Aggregation results in the red shift of the SPR (from 520 nm to  $\sim 600$  nm) and a visible red-to-purple color transition of the particles in solution. Reproduced with permission from ref 78. Copyright 2011 John Wiley & Sons, Inc. (C) Compared to duplexes of free-strand DNA, which dissociates over a broad temperature range, the melting transitions of SNAs are sharp and occur over a very narrow temperature range due to the cooperative binding of the nucleic acids in the SNA shells. Reproduced with permission from ref 6. Copyright 2005 American Chemical Society. (D) Melting temperatures of duplexes labeled with a quencher (green) and a fluorophore (purple), duplexes on silica particles ( $\sim 100$  nm in diameter), and SNA–Au NP conjugates (13 nm in diameter). The melting transition of free and silica particle-bound duplexes are similar because the density achieved on silica particles is typically low (1/30th that of the SNA–Au NP conjugates). The melting transition of SNA–Au NP conjugates occurs at higher temperatures due to the properties of the dense SNA shell.

to a surface, for example in a chip-based assay,<sup>40,77</sup> although the transition is not as narrow as one observes in the aggregates. Experimentally, this phenomenon is observed for SNAs without particle cores as well.<sup>20</sup> The sharpness of the melting transition can be quantified mathematically by calculating the full width at half-maximum (fwhm) of the first derivative of the melting curve. Typical fwhm values for typical AT-rich duplexes, 10 bases in length, are  $\sim 10$  °C, while fwhm values for the transitions observed for hybridized aggregates of SNA conjugate structures formed from the same oligonucleotides are in the range of 1–3 °C. As will be discussed in section 8, the narrow melting transition observed for SNA nanostructures is important in their applications for diagnostics where a single oligonucleotide base-pair mismatch is enough to perturb the melting behavior of the aggregate, allowing it to be differentiated from the aggregates made from fully complementary duplex structures.

One explanation for the increase in melting temperature of the aggregate compared to the free strands is that the higher surface density of oligonucleotides on the particle surface gives rise to a greater number of interparticle connections that are collectively stronger and present at a higher effective concentration compared to DNA duplexes free in solution. Thus, decreasing the number of recognition strands on the particle surface (either through the addition of nonrecognition “diluent” strands or by decreasing the extent of chemisorption of the recognition strand during the functionalization/salting step) results in a broader melting transition that begins at a lower temperature. Additionally, the high local salt environment in the area surrounding the NP, in certain cases, imparts greater stability to the duplexes and contributes to the increase in melting temperature (Figure SD).<sup>79</sup> High local salt concentration is also believed to be responsible, in part, for the cooperative, narrow melting transition. At the start of the melting transition, when strands begin to dehybridize, there is a simultaneous decrease in the local salt concentration that decreases the melting temperature of the remaining strands. We and the Schatz group have provided both experimental and theoretical evidence to support a “shared ion cloud” theory in which cooperativity in oligonucleotide melting transitions arises from the dielectric environment of duplexed strands in close proximity to one another.<sup>80,81</sup> Nguyen and co-workers have provided further experimental evidence for this theory using a molecular system in which sharp melting transitions were observed for systems containing only a few oligonucleotides, oriented in a manner such that shared ion interactions could take place.<sup>82,83</sup>

Importantly, the characteristic sharp melting of hybridized SNAs is a direct result of the collective behavior of the dense monolayer of oligonucleotides in the SNA shell. Indeed, subsequent studies have shown that the narrow melting transitions observed initially for the SNA–Au NPs are not core-dependent, but rather characteristic of all SNA–NP conjugates including QDs,<sup>44</sup> SPIONs,<sup>43</sup> Ag NPs,<sup>42</sup> and coreless SNAs,<sup>20</sup> as well as anisotropic prisms, rods, and rhombic dodecahedra.<sup>84,85</sup> The collective interactions of DNA can bring particles together even if the individual binding strength on a per strand basis is weak. This effect results in “three-dimensional hybridization”, where the SNAs as single multi-strand entities hybridize together.<sup>86</sup> For example, linear strands that are complementary by three base pairs will not hybridize in solution (e.g., 5'-GCG-3' and 5'-CGC-3'). However, if particles are functionalized with strands terminated with the identical sequences, hybridization will occur and particles will aggregate. This effect is more prominent with larger NPs. For example, when 150 nm particles are aggregated, the total number of DNA linkages between particles is much greater than the number between aggregated 5 nm particles (hundreds compared to less than 10). Therefore, even a single base-pair interaction can cause aggregation of particles of larger sizes.<sup>86</sup> The fact that such weak interactions can aggregate particles is an important consideration for sequence design of SNA conjugates. For instance, if a researcher intends to synthesize particles for an application in gene regulation or diagnostics, the sequence should be checked for self-complementarity; indeed, even a few bases can cause unanticipated and undesirable particle aggregation.

Interestingly, cooperative binding is not limited to canonical DNA binding. DNA binding modes that rely on G-quadruplex formation can also be accessed by the SNA structure.<sup>87</sup> One

would normally expect the two sequences, 5'-CCCC-3' and 5'-GGGG-3', to have one melting transition. However, because the G-rich sequence can form quadruplexes, particles functionalized with these strands exhibit two melting transitions.<sup>88</sup> Furthermore, this has implications for sequence design; one should not synthesize SNAs with oligonucleotides terminated with G bases.

In some respects, DNA bases are to DNA strands as DNA strands are to SNA conjugates. This hierarchy makes interesting 3D modes of hybridization possible that are not expected if one only considers the dynamics of single linear strands in isolation. These considerations are exceedingly important, and only through understanding these fundamental polyvalent interactions of SNAs can researchers realize new ways of making macroscopic materials from these nanoscale building blocks.

## 6. NANOPARTICLE ASSEMBLY AND CRYSTALLIZATION PROGRAMMED WITH SPHERICAL AND OTHER 3D NUCLEIC ACID NANOSTRUCTURES

The SNA conjugate is a versatile and chemically programmable synthon that can be used to construct higher ordered materials, in particular colloidal crystals. Indeed, early work showed how linker strands could be used to assemble different particle building blocks into polymeric materials with unusual properties that derived from placement of the particles within such assemblies.<sup>1,89</sup> The property changes that accompanied such assembly events became the basis for many new nucleic acid-based diagnostic systems (section 8). In addition to diagnostic applications, subsequent work began to show how one can force the assembly of such particles into colloidal crystals exhibiting short-range order, where interparticle distances can be modulated by linker length.<sup>89</sup> Further work has shown the ability to create complex discrete structures, such as asymmetrically functionalized particles and programmably assembled clusters.<sup>90–92</sup> These works provided some of the fundamental knowledge necessary for the discovery in 2008 by our group and the Gang group (using related techniques) that SNA-modified Au NPs could be crystallized exclusively into either face-centered cubic (fcc) or body-centered cubic (bcc) lattices through judicious choice of linker strands and annealing (Figure 6A).<sup>93,94</sup> A key insight was that the weak binding interactions of short DNA linker sequences combined with the polyvalent cooperative binding observed for SNA conjugates (section 5) allows the system to self-correct defects and transform from an initial disordered aggregate into an energetically favored crystalline arrangement. Specifically, the large number of linkages can hold the aggregate together, yet because they are weak individually, they can hybridize and dehybridize dynamically. Thus, annealing an aggregate at a temperature slightly below its melting temperature provides the thermal energy required for the transition from a disordered to an ordered structure to take place. The NP superlattices synthesized using SNA conjugates exhibit a very high degree of crystalline order, as demonstrated by small-angle X-ray scattering (SAXS). SAXS is the primary characterization method for such structures because these superlattices typically exist only under conditions where DNA duplexes are stable, namely, aqueous saline solutions. As a secondary structural characterization technique to complement SAXS, we have recently developed a resin-embedding method for visualizing the NP superlattices by transmission electron microscopy

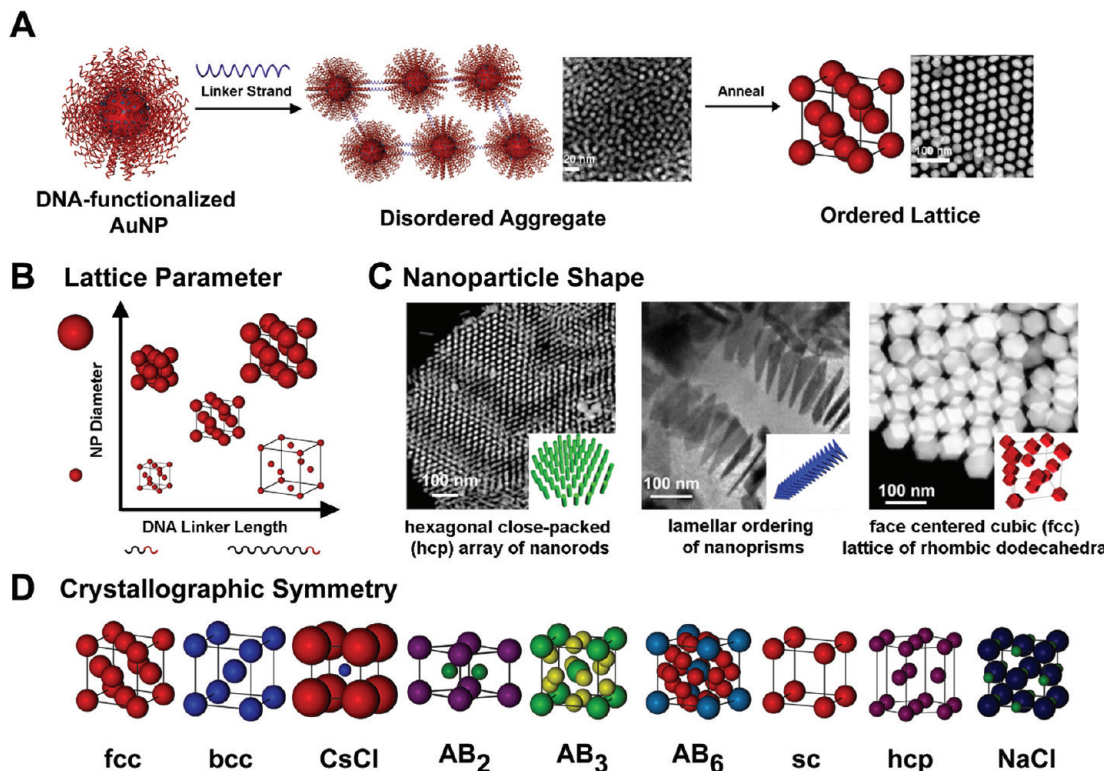


**Figure 6.** (A) Schematic illustration of DNA-programmable nanoparticle assembly into ordered superlattices (fcc lattice shown). TEM images show the transition from disordered aggregate (10 nm Au NPs shown) to ordered lattices (30 nm Au NPs shown) after annealing at a temperature slightly below the melting temperature of the aggregate. TEM image of the ordered NPs reproduced with permission from ref 95. Copyright 2011 The American Association for the Advancement of Science. The programmable parameters that can be controlled using this technique are (B) the lattice parameter, which can be tuned by using different linker lengths and NP diameters (figure not to scale), (C) NP shape, where directional bonding of different anisotropic NPs leads to a variety of one-, two-, and three-dimensional lattices, and (D) crystallographic symmetry, which can be controlled by linker lengths, linker sequences, and molar ratios of particles. Panel B is reproduced with permission from ref 85. Copyright 2011 Nature Publishing Group.

(TEM).<sup>85,95</sup> These initial studies highlighted the use of DNA as a robust and programmable assembly tool for the formation of highly ordered NP superlattices and further demonstrated the potential materials applications made possible by the unique properties of SNA conjugates.

In addition to the reversible binding of short DNA sequences to the SNA shell, the ratio of DNA length to particle core size was found to be an important factor for determining whether a system reorganizes into a crystalline state. For fcc-type systems, a “zone of crystallization” was identified, as defined by this ratio, where ordered crystals are observed only when working within the constraints of the DNA length and particle core size parameters.<sup>96</sup> These boundaries in the phase diagram exist because the ratio of DNA length to NP diameter affects both the number of stable DNA linkages that can be formed between particles and the rate at which those linkages are broken ( $k_{\text{off}}$ ) and re-formed ( $k_{\text{on}}$ ) during the reorganization process. At low ratios of DNA length to NP diameter, higher relative energetic penalties associated with DNA bending and stretching that are required to maximize the number of DNA connections between particles prevent crystal formation (it is harder to bend shorter duplexes than longer ones). For long, flexible DNA linkages between particles (>100 bp), i.e., high ratios of DNA length to NP diameter, a decrease in the local concentration of both salt and DNA “sticky ends” (short recognition elements at the terminus of the DNA sequence) results in a greater  $k_{\text{off}}$  for DNA binding between particles and disfavors the reorganization process toward crystal formation.

In related work, Gang and co-workers adjusted two distinct variables, the DNA linker length and the number of DNA connections, to generate a phase diagram delineating the boundary between crystalline (bcc-type) and disordered aggregates.<sup>97</sup> It was observed that formation of ordered lattices required a greater number of linkages for longer linkers, most likely due to the destabilizing effects of lower effective linker concentrations on the reorganization process. Both phase diagrams are based upon the important concept that high-density DNA and the cooperative and reversible binding of the DNA linkages are required in the transformation from disordered aggregates to ordered superlattices.

One of the key advantages offered by DNA-mediated assembly is that parameters such as particle diameter, shape (Figure 6B,C), DNA length, and sequence can be tuned independently. This provides a means to synthesize colloidal crystals with lattice parameters that can be controlled and predicted with nanometer precision (calculated rise per base pair =  $0.255x + 11.1$  nm, with  $R^2 = 0.987$ , where  $x$  is the total number of bases between Au NPs; this rise per base differs from that of canonical B-form DNA).<sup>98</sup> The packing density of the NP lattice is controlled by the sequence of the linker sticky ends: a self-complementary linker sequence (5'-GCGC-3') allows every particle to bind to its nearest neighbor and favors the formation of a close-packed fcc lattice. In contrast, a pair of non-self-complementary linkers (e.g., 5'-TTCCTT-3' and 5'-AAGGAA-3') produces two particle types, “A” and “B”, and favors the formation of the non-close-packed bcc lattice if the

particles are added in equal amounts.<sup>93</sup> In addition to a binary lattice consisting of particles that all have the same inorganic core, where the two particle types are differentiated by the identity of the DNA sequence, a bcc lattice composed of "A"-type Au NPs and "B"-type QDs has also been synthesized.<sup>99</sup>

This system has evolved to one that offers a high level of predictability based upon a set of design rules that we recently introduced.<sup>95</sup> The seven rules, which are summarized below but explained in detail elsewhere,<sup>95,153</sup> are as follows:

- (i) The most stable crystal structure maximizes all possible types of DNA hybridization interactions.
- (ii) For a system where all SNA–Au NPs possess the same hydrodynamic radii, each SNA–Au NP in the thermodynamic product will maximize the number of nearest neighbors with which it can form DNA connections.
- (iii) When two lattices are of similar energetic stability, the kinetic product can form if the rates of DNA linker de- and rehybridization are slowed.
- (iv) The hydrodynamic radii of the SNA–Au NP conjugates, rather than the size of the constituent Au NPs or the length of the oligonucleotides, dictate their assembly and packing behavior.
- (v) For binary systems, the size ratio and DNA linker ratio between particles dictate the thermodynamically favored crystal structure.
- (vi) Two systems with the same size ratio and DNA linker ratio produce the same thermodynamic product.
- (vii) Hollow SNAs can be used as spacer elements within nanoparticle superlattices to access symmetries not accessible with core-filled structures.<sup>153</sup>

These six rules, which have been formulated on the basis of experiments and modeled phase diagrams, have been used to construct over 50 SNA–Au NP superlattices with nine distinct crystallographic symmetries (Figure 6D). In addition to fcc and bcc lattices, superlattices with hexagonal close-packed (hcp), cesium chloride (CsCl), AB<sub>2</sub> (isostructural with aluminum diboride), AB<sub>3</sub> (isostructural with Cr<sub>3</sub>Si), AB<sub>6</sub> (isostructural with the alkali-fullerene complex Cs<sub>6</sub>C<sub>60</sub>), sodium chloride (NaCl), and simple cubic (sc) symmetry have been synthesized. With the exception of hcp, all are assumed to be thermodynamic products, made by annealing the programmed structures at a temperature near the onset of the melting transition. The rules are analogous to Pauling's rules for determining the packing behavior of complex ionic solids,<sup>100</sup> but in many ways afford greater predictability and tunability due to the ease with which DNA interactions can be programmed.

## 7. MOVING BEYOND SPHERICAL CONJUGATES TO OTHER FORMS OF 3D NUCLEIC ACIDS

In addition to size-dependent properties, many physical and optical properties are dependent upon nanoparticle shape, and some are unique to NPs exhibiting anisotropy (e.g., rods, prisms, cubes). For example, the plasmon resonances of such structures are highly dependent on their shape and aspect ratio.<sup>101,102</sup> The diverse properties of anisotropic NPs have been reviewed in detail elsewhere;<sup>103–106</sup> here, we will focus solely on the emergent properties of DNA-functionalized anisotropic particles in the formation of nonspherical 3D nucleic acids (Figure 7A).

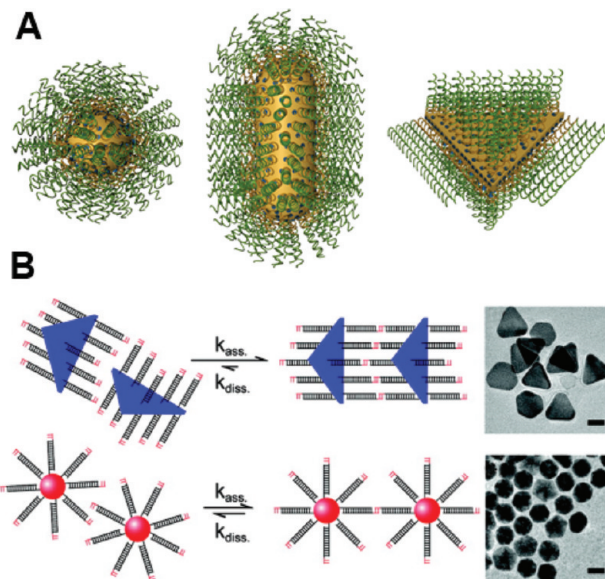


**Figure 7.** (A) Illustration of 3D SNA conjugates formed from different particle templates: spheres, rods, and triangular prisms. (B) Schematic demonstrating the difference between anisotropic 3D nucleic acid hybridization and SNA hybridization. Reproduced with permission from ref 115. Copyright 2011 American Chemical Society.

Because the synthesis conditions for anisotropic particles are often distinct from those of spherical nanostructures, DNA surface-immobilization must be tailored for each of these particle types. For instance, many anisotropic Au nanostructures are synthesized in the presence of the capping agent cetyl trimethylammonium bromide (CTAB).<sup>107–109</sup> Because CTAB is a positively charged surfactant, it effectively complexes and sequesters the DNA, preventing it from adsorbing to the Au NP surface. Therefore, it must be removed by iterative centrifugation and washing steps before DNA functionalization can occur in an analogous way to how spherical Au NPs are functionalized.<sup>84,85</sup>

Like their spherical counterparts, these anisotropic particles have unusual and useful properties due to both their inorganic cores and dense surface coating of oligonucleotides. For example, the size- and shape-tunable near-infrared (NIR) absorption of many anisotropic particles has utility in the development of diagnostic and imaging tools. We and others have demonstrated light-mediated methods to release DNA from anisotropic NPs either through breakage of the Au–S bond<sup>110</sup> or through dehybridization of complementary DNA strands via local photothermal heating.<sup>110–114</sup> Because the size, and therefore the resonance wavelength, of these anisotropic particles can be finely controlled, one can selectively dehybridize strands from a given particle type within a mixture simply through appropriate choice of the laser irradiation wavelength.<sup>112</sup> This combination of the plasmonic properties of the NPs and the thermal properties of the anchored DNA strands allows one to wield spatiotemporal control over the local concentration and bioavailability of oligonucleotides in biological systems.

The degree of anisotropy associated with a particle scaffold can dramatically influence the collective behavior of the oligonucleotides comprising 3D nucleic acids. In recent work, we have shown that the binding affinity between complementary DNA-functionalized triangular nanoprisms is several million times higher than that of SNA–Au NP conjugates with

similar oligonucleotide loadings.<sup>115</sup> As the sphericity of a structure decreases, more connections between 3D nucleic acids can be supported through greater interparticle surface contact, such as between two flat extended surfaces (Figure 7B). This geometry increases the effective local concentration of oligonucleotides available for binding, which increases the “on” rate of hybridization. Additionally, the binding interactions between flat surfaces impart less conformational stress on the hybridized duplexes as compared to those that bridge SNAs. Taken together, these factors form the basis for beginning to understand the “valency” of nonspherical 3D nucleic acids. Furthermore, these striking observations recapitulate the notion that the orientation and density of nucleic acids at the nanoscale are unique parameters that can be tailored to obtain nanostructures with a wide range of unusual and novel chemical and physical properties.

In the areas of materials synthesis and programmed colloidal crystallization, nonspherical 3D nucleic acid nanostructures provide access to NP superlattices with greater structural diversity than can be achieved with isotropic NPs. The introduction of the concept of NP shape into the DNA-based assembly methodology imparts a kind of “nanoparticle valency”, where directional hybridization interactions between particles allow for the formation of one-, two-, and three-dimensional superlattices that would be difficult, if not impossible, to synthesize with other assembly or lithography methods.<sup>85</sup> These directional interactions occur because DNA base-pairing between anisotropic particles is favored along directions that maximize parallel face-to-face interactions between particles. Thus, following DNA functionalization, nanoprisms assemble into 1D arrays along the prism faces, nanorods assemble into 2D sheets with hexagonal close-packed (hcp) ordering, and rhombic dodecahedra assemble into 3D fcc lattices (Figure 6C). Analogous to the unique physical properties possessed by anisotropic NPs over their spherical counterparts, other forms of 3D DNA allow access to an entirely new design space for NP superlattices that is distinct from what is achievable with SNAs alone. Finally, efforts to face-selectively functionalize particles with different oligonucleotides<sup>84,90,91</sup> will dramatically increase valency control, the synthetic tunability of this system, and the sophistication of the types of materials and crystals that can be constructed.

## 8. DIAGNOSTICS

During the initial studies of the SNA–Au NP conjugates, we recognized immediately that their reversible melting behavior over a narrow temperature range and their corresponding hybridization-dependent optical changes could be useful for high-selectivity detection platforms (*vide infra*). Since that time, SNA nanostructures have been used to develop a wide variety of *in vitro* and intracellular molecular diagnostic systems for a range of analytes. These include solution-based colorimetric<sup>4</sup> and chip-based scanometric systems for nucleic acid,<sup>5</sup> protein,<sup>71</sup> small-molecule,<sup>116</sup> and metal-ion-based targets<sup>117</sup> (*vide infra*). The utility of SNA structures in diagnostic applications arises in part from both the properties of the SNA’s polyvalent oligonucleotide shell and the physical and chemical properties of the inorganic core. Taken together, these two components yield probes that offer significant advantages over molecular counterparts.

In a typical colorimetric assay using SNA–Au NP probes, a target entity is captured by two distinct sets of Au NPs, each functionalized with a strand programmed or chemically

modified to impart specificity to its target, such that the presence and subsequent capture of target triggers the reversible aggregation of the Au NP probes (Figure 5A,B). This process results in a visible red-to-purple color transition due to a red shift in the SPR of the Au NPs, which can be monitored by eye or spectroscopically. Significantly, an aggregate formed from a perfectly complementary target nucleic acid sequence exhibits a very narrow melting transition (compared to duplex DNA) and can readily be differentiated from target strands containing a single base-pair mismatch, insertions, or deletions.<sup>40</sup> This observation is clinically relevant because single nucleotide polymorphisms (SNPs) play a role in many diseases.<sup>118</sup> Furthermore, the high extinction coefficient of Au NPs allows one to detect targets at lower concentrations than conventional molecular dyes. To date, colorimetric detection systems designed with the appropriately functionalized SNA conjugates have been used to quantitatively measure the concentrations of nucleic acids,<sup>4,73</sup> enzymes,<sup>119</sup> small-molecule targets (via aptamers),<sup>120</sup> enzymes,<sup>121</sup> known DNA-binding molecules (e.g., 4',6-diamidino-2-phenylindole (DAPI), ethidium bromide),<sup>122</sup> Hg<sup>2+</sup> ions,<sup>123</sup> copper ions (Cu<sup>+</sup> and Cu<sup>2+</sup>),<sup>69</sup> and other metal ions.<sup>124</sup> Particles do not need to be directly cross-linked by a target molecule to achieve target-specific aggregation. For example, Sato et al. have developed a system that takes advantage of conformational changes of the SNA shells when they bind to their targets. At high salt concentrations, particles will rapidly aggregate when they bind their complements due to reduced repulsive interactions between particles.<sup>54</sup> In principle, solution-based colorimetric detection strategies can be used to detect any target that has the ability to bring plasmonic NPs together through interactions with suitably designed oligonucleotides. Reverse colorimetric detection platforms, whereby the presence of target triggers the dispersion of aggregated particles and a concomitant purple-to-red transition, have also been developed by Lu and co-workers.<sup>125</sup> In these systems, SNA–Au NPs are aggregated in the presence of a DNAzyme that can be cleaved upon binding of the appropriate target, which results in particle dispersion.<sup>126</sup> Finally, other systems that cause a change in the physical properties of the inorganic core of SNAs, based upon magnetic,<sup>127</sup> Raman,<sup>128</sup> or fluorescent signals,<sup>67</sup> also have been developed.

The ability to differentiate SNPs by NP-based colorimetric detection was a significant advance in molecular diagnostics. In 2000, to increase the sensitivity offered by this system, we developed a chip-based method called the scanometric assay where the capturing of a desired target results in the immobilization of the Au NP probes onto a functionalized glass slide in a three-component, sandwich-type assay (Figure 8A).<sup>5</sup> Additionally, this assay utilized the catalytic properties of the Au NPs, namely its ability to promote the reduction of silver(I) in the presence of hydroquinone, as a method for signal amplification. Silver-coated Au NPs could then be readily detected by traditional flat-bed scanners, whereby the presence of more immobilized NPs, and hence more captured targets, resulted in a greater light scattering. A second gold<sup>71</sup> or silver deposition<sup>5</sup> step was shown to increase the limit of detection (LOD) offered by this assay, though subsequent depositions did not improve the LOD due to increased background signals for all target concentrations (Figure 8B, C). Since its discovery in 2000, the scanometric assay has been extended to proteins,<sup>129</sup> commercialized, FDA-cleared, and used in a variety of highly sensitive molecular diagnostic technologies.<sup>6,30,100</sup> In

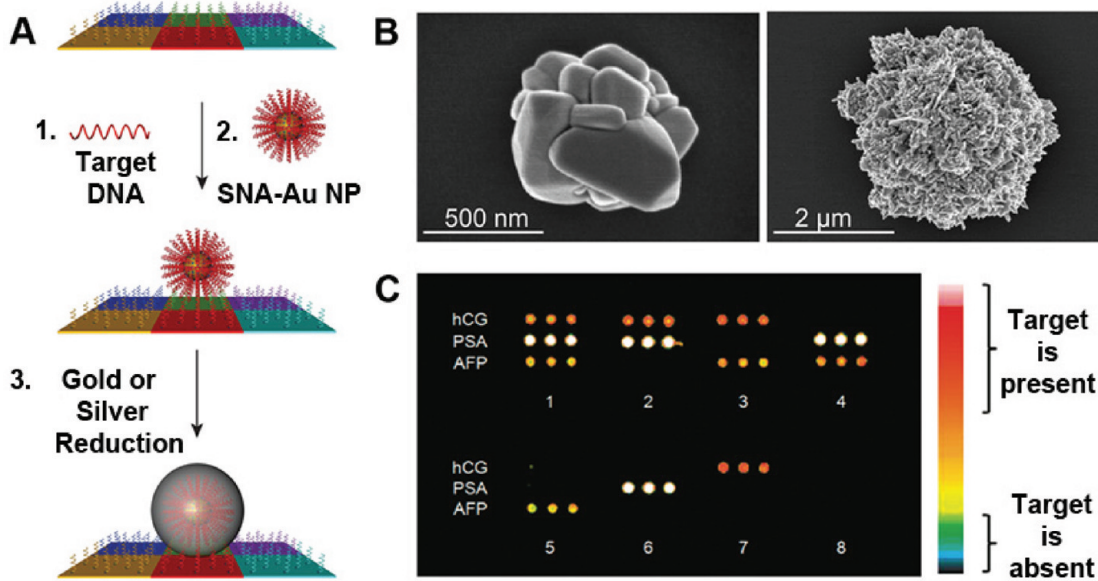


**Figure 8.** (A) Schematic illustration of a scanometric detection assay. A chip is synthesized with capture strands for a number of different targets. The targets will hybridize to the appropriate spots if they are present. The chip is then exposed to a solution of SNA–Au NP probes, which will hybridize to the appropriate targets if they are on the chip. The binding of the SNA–Au NP probes can be visualized by reducing metal ions (Ag or Au) on the NP cores, which creates a macroscopic structure. The SNA probes can be modified with many recognition elements, such as antibodies, which allows for the detection analytes beyond nucleic acid targets. (B) Large macroscopic structures created by reduction of Ag (left) and Au (right). The Au is a better signal enhancer due to its mechanism of reduction, which results in larger macroscopic particles. (C) Read-out of a scanometric detection assay. If the target is present, the macroscopic structure can be detected via light scattering and a conventional optical flat-bed scanner. A bright spot indicates that target is present, and the signal intensity permits quantification of target concentration. Panels B and C reproduced with permission from ref 71. Copyright 2009 American Chemical Society.

2009, we developed an analogous scanometric immunoassay using antibody-modified SNA–NP conjugates where the target in this case was prostate-specific antigen (PSA) rather than DNA.<sup>71</sup> This study also showed that using gold deposition steps increased the LOD by 2 orders of magnitude from 30 fM to 300 aM, compared to the same assay using an equal number of silver deposition steps.

Strategies that rely on more sophisticated versions of SNA conjugates, such as the biobarcode assay,<sup>130</sup> have been introduced. With such assays, a NP probe is designed with “barcode” DNA strands that are hybridized to an SNA conjugate functionalized with strands complementary to the barcode sequence as well an antibody for an antigen of interest (e.g., PSA). In the barcode assay, rather than directly detecting the antigen molecules, signal amplification is effected by releasing the barcode DNA strands, post antigen sequestration and isolation, followed by their detection with the scanometric assay. Further signal amplification is possible by using polymerase chain reaction (PCR) to increase the copies of the barcode DNA, though the PCR-less technique using larger Au NPs (30 nm) was shown to effectively detect PSA at attomolar concentrations. Variants of this assay have been used to study clinical disease states including Alzheimer’s disease<sup>154</sup> and prostate cancer.<sup>155</sup>

## 9. SPHERICAL NUCLEIC ACIDS AS SINGLE-ENTITY GENE REGULATION CONSTRUCTS

Regulation of gene expression with synthetic oligonucleotides has led to fundamental breakthroughs in the understanding of intracellular function<sup>131</sup> and may lead to viable treatment options for genetic-based diseases, such as many forms of cancer and neurological disorders.<sup>132,133</sup> However, the delivery of synthetic nucleic acids to disease sites and across cell

membranes is still a major challenge for gene regulation therapies (antisense DNA and siRNA). Indeed, Nature has created a defense network for foreign nucleic acids. For example, since nucleic acids are negatively charged, they cannot easily cross the negatively charged cell membrane. Furthermore, they are rapidly degraded by nucleases and activate the innate immune response in cells. Historically, researchers have required the use of transfection agents, such as cationic polymers,<sup>122,134,135</sup> liposomes,<sup>136</sup> and modified viruses,<sup>137</sup> to shuttle the nucleic acids through the negatively charged cellular membrane and shield them from enzymatic degradation. Unfortunately, these methods are not ideal for systemic delivery because of their inability to be degraded naturally, severe immunogenicity, and toxicity at high concentrations (Table 1).<sup>138,139</sup> The most widely used agents, cationic polymers, complex the nucleic acid material and neutralize its charge, allowing the hybrid material to breach cellular membranes by fusing with them.<sup>140</sup> SNA constructs provide an alternative in this regard since, despite their large negative charge (zeta potential < -30 mV), they have been found to enter cells in very high numbers, without the need for ancillary transfection agents.<sup>15</sup> Additionally, SNA–NP conjugates have a unique set of properties specific for intracellular applications, such as high binding coefficients for complementary DNA and RNA (*vide supra*),<sup>39</sup> nuclease resistance,<sup>41</sup> minimal immune response,<sup>141</sup> no observed toxicity,<sup>74</sup> and highly effective gene regulating capabilities.<sup>17,20,142</sup> Again, all of these properties derive from the 3D structure of the densely packed, highly oriented oligonucleotide shell on the surface of the particles.

It has been shown that the dense DNA monolayer is primarily responsible for cellular uptake, as bare citrate-stabilized particles (the only other component in the system) or particles without DNA but passivated with BSA show orders

of magnitude lower cellular uptake.<sup>74,143</sup> Furthermore, this uptake is universal for any NP functionalized with a dense shell of DNA ( $\sim 20 \text{ pmol}/\text{cm}^2$ ). Indeed, conjugates made from other cores, such as iron oxide NPs, also show high cellular uptake without transfection agents.<sup>43</sup> One of the most convincing pieces of evidence for the importance of this surface structure/uptake relationship comes from studies of coreless SNAs (Figure 9).<sup>20</sup> These particles, which are as close as one can get

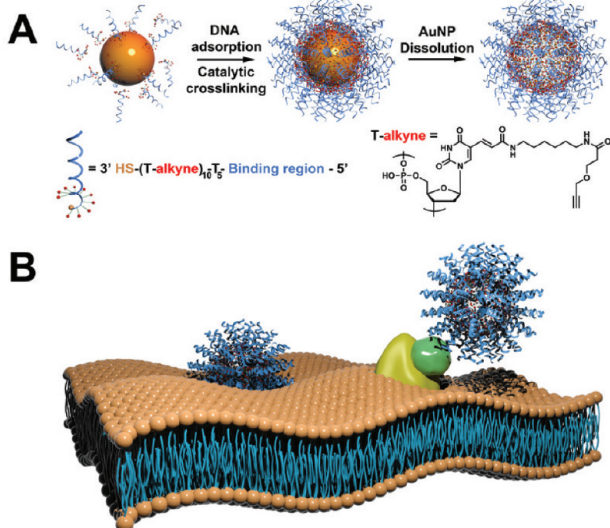


**Figure 9.** (A) Synthesis of hollow SNAs. Alkyne-modified oligonucleotides are adsorbed onto Au NPs, which then catalyze the cross-linking of the alkyne groups. After purification from excess oligonucleotides, the cores are dissolved with potassium cyanide, which yields hollow SNAs. (B) Schematic of hollow SNAs interacting with scavenger receptors in the cell membrane, which induces endocytosis of the particles. Reproduced with permission from ref 20. Copyright 2011 American Chemical Society.

to pure SNA, are composed only of cross-linked nucleic acids, which are oriented in the same fashion as SNA–Au NP conjugates. They can be synthesized from modified forms of DNA or RNA and exhibit many of the same properties of inorganic NP-based SNAs. Furthermore, they anticipate concerns about the potential toxicity of the inorganic gold core.

Importantly, SNAs (with or without an inorganic core) are capable of rapidly entering every cell type tested thus far (over 50), including primary cells, with the exception of mature red blood cells.<sup>15</sup> Inductively coupled plasma or radiolabeling allows for quantification of the number of particles that enter each cell, which often exceeds millions. This seemingly universal uptake phenomenon is facilitated in part by membrane-bound scavenger receptors,<sup>144</sup> which are known to mediate endocytosis of specific polyanionic ligands, such as oligonucleotides,<sup>145</sup> including phosphorothioate variants.<sup>146</sup> In a proposed mechanism, serum proteins (such as BSA) first adsorb to the SNA's oligonucleotide shell, slightly inhibiting uptake of particles.<sup>74</sup> Next, the serum proteins are displaced by scavenger receptors at the cell surface, a process that initiates endocytosis of the particles. By inhibiting these receptors with their natural agonists, such as poly-inosine (I) and fucoidan, the uptake of SNAs is significantly reduced.<sup>31</sup> The interaction between the dense nucleic acid shell of SNAs and cell membranes governs this uptake phenomenon; higher densities result in higher uptake of SNAs (Figure 10A).

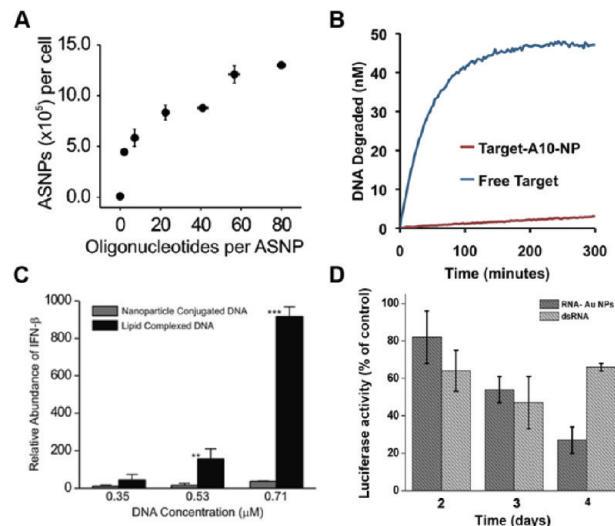


**Figure 10.** (A) Oligonucleotide density determines the cellular uptake numbers of SNA–NP conjugates; higher densities result in more particles per cell. Reproduced with permission from ref 74. Copyright 2007 American Chemical Society. (B) SNAs are degraded much more slowly by nonspecific serum nucleases compared to duplexes of the same sequence. In an *in vitro* experiment where the concentration of nuclease was at elevated levels to shorten experimental time windows, less than 10% of the SNA duplexes were degraded after 300 min. In contrast, all of the free duplexes are completely degraded in 200 min. Reproduced with permission from ref 148. Copyright 2011 American Chemical Society. (C) Relative amounts of interferon- $\beta$  produced after transfection with SNA–Au NP conjugates and lipoplexed DNA. Reproduced with permission from ref 141. Copyright 2009 American Chemical Society. (D) Gene knockdown of siRNA-based SNA conjugates is more persistent than with lipoplexed siRNA. Studies show that this effect is likely due to the higher stability of SNAs in biological media as compared to free duplexes. Reproduced with permission from ref 17. Copyright 2009 American Chemical Society.

Beyond being able to enter cells easily without transfection agents, SNAs also possess important properties for function within a cell. The SNA's dense oligonucleotide shell is capable of deactivating enzymes in close proximity to the conjugate due to the high local sodium ion concentration.<sup>79,147</sup> SNA conjugates exhibit remarkable serum and intracellular stability because of their ability to deactivate many nucleases in this way.<sup>41</sup> This property is exceedingly important in the context of nucleic acid delivery and gene regulation because oligonucleotides are otherwise rapidly degraded by such nucleases. In buffer, the rate of degradation of SNA (duplexes) by many nucleases is  $\sim 4$  times slower than that of free duplexes, primarily due to a decreased rate of hydrolysis. In serum, however, this rate difference is drastically increased because nonspecific serum proteins can adsorb to the particles' surface, which is hypothesized to block and further inhibit nucleases from accessing the surface strands (Figure 10B).<sup>148</sup> Furthermore, SNA conjugates can evade proteins that recognize foreign nucleic acid material, thereby avoiding the innate immune response that would otherwise be activated by foreign nucleic acids.<sup>141</sup> Thus, despite the very high number of NPs that can enter the cells, the immune response (as measured by the interferon- $\beta$  level) is significantly lower ( $\sim 25$  times lower) as compared to that of DNA transfected by conventional polymeric agents (Figure 10C).

Once inside the cell, SNA conjugates can carry out tasks related to their chemically programmed oligonucleotide shell.

For example, if the shell is composed of DNA targeted for mRNA, the structures can regulate gene expression via the antisense pathway.<sup>15</sup> RNA conjugates also have been synthesized, which can regulate gene expression through the RNAi pathway.<sup>17</sup> These conjugates have been shown to be extremely potent, with only picomolar concentrations needed to see knockdown in some cases. Interestingly, the knockdown of mRNA and protein levels by SNAs is more persistent than knockdown via nucleic acids delivered with cationic agents (Figure 10D).<sup>15,17</sup> This is likely due to the intracellular stability of SNAs discussed above. Additionally, the stability of the nucleic acid shells allows for attachment and delivery of other chemical agents, such as metal complexes. For example, platinum(IV) prodrugs have been covalently attached to SNA–Au NPs to create a potent delivery vehicle for cisplatin.<sup>67</sup> Once internalized in the cells with the SNA–Au NPs, the platinum(IV) complexes are reduced to a cytotoxic Pt(II) species and released into the cytosol through reductive elimination of their axial ligands. On a per platinum basis, the Pt–SNA–Au NP conjugates were significantly more effective than cisplatin or the prodrug alone. Additionally, drugs that are not soluble and thus difficult to administer, such as paclitaxel, can be conjugated to the SNA shell.<sup>72</sup> This strategy takes advantage of the high stability and high cellular uptake of SNAs. The solubility of paclitaxel can be increased by over 50 times, and when attached to SNA–Au NP conjugates, the drug exhibits lower IC<sub>50</sub> values (4–10 times) compared to free drugs. The attachment of drugs to SNAs may become a general method to deliver drugs and other chemical agents for disease applications.

The high cellular internalization of SNAs is indeed promising for the field of gene regulation; however, their indiscriminant uptake may pose challenges for targeting *in vivo*. Indeed, in their present state of development they are ideal for local delivery applications where targeting can be done at the genetic level. Unlike chemotherapy, where all cells are potentially subject to the cytotoxic effects of drugs, SNAs target the genetic expression profiles of cancerous cells only. Nevertheless, the chemical tailorability of the nucleic acid shell provides an ideal scaffold for chemical modification. For example, one can envision the covalent attachment of targeting moieties on the periphery of the shell through modified bases and bioconjugation. Alternatively, one could hybridize oligonucleotides with targeting “cargo” in a relatively straightforward fashion. SNAs can be synthesized over a range of particle sizes, which suggests that they may be tailored for specific disease types.<sup>149</sup> Collectively these strategies provide a blueprint for developing a wide variety of new therapeutic candidates based on SNAs.

Taken together, these observations challenge the notion that one needs an auxiliary agent to deliver oligonucleotides to cells. Previous work has focused on how to tailor the carrier to be compatible with biological systems to minimize its toxicity and immunogenicity, while maximizing efficiency. Now, one can consider SNA and other 3D forms of nucleic acids as single-entity gene regulation agents, capable of freely entering a wide variety of cell lines and effecting gene regulation in a very potent manner (Figure 11).

## 10. COMBINED INTRACELLULAR DIAGNOSTICS AND IMAGING

SNAs are also leading to intracellular diagnostic and imaging tools and platforms. Fluorophore tags can be attached to them, making it straightforward to locate and image particles in

## Different Paths to Gene Regulation

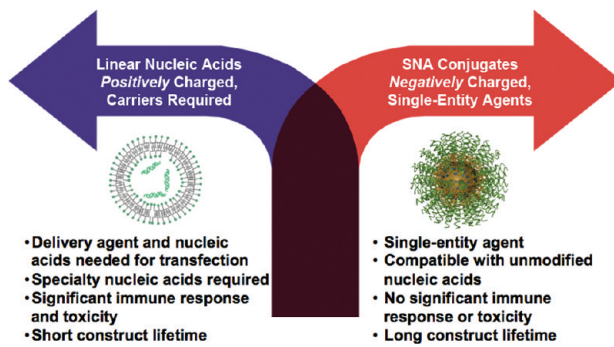


**Figure 11.** SNAs offer a different paradigm for gene regulation. Negatively charged nucleic acids do not need to be precomplexed with synthetic positively charged carriers to enter cells and effect gene regulation. If the nucleic acids are densely oriented at the nanoscale, they enter cells in high numbers, resist degradation, exhibit nuclease resistance, show no apparent toxicity, and do not activate the innate immune response.

cells.<sup>15</sup> Furthermore, by attaching gadolinium chelates to such particles, one can synthesize multimodal particles useful for magnetic resonance imaging techniques.<sup>50</sup> As discussed in section 8, SNAs are highly specific for target sequences and can thus be used to detect and measure the concentration of over- or under-expressed mRNA in cells that may indicate disease or be representative of a particular cell state (e.g., cancerous vs noncancerous). Static measurements of such disease markers are important; however, the ability to measure and quantify activity dynamically (e.g., in response to stimuli) on a per cell basis can give valuable information that a measurement on a bulk cell sample cannot capture. SNA conjugates provide a solution in this regard, as they can enter cells autonomously with no significant disruption to normal cellular function and they resist enzymatic degradation. Moreover, they can be designed to target only specific genes of interest (section 9). In the case of Au NPs, one can take advantage of the highly efficient fluorescence quenching ability of the gold core to create a dynamic fluorophore-based “off-on” system that responds to varying levels of mRNA expression in the cell.<sup>11</sup> These probes, termed “nanoflares”, are designed with strands complementary to disease-related mRNA (~18 bases long), such as survivin, and a fluorophore-labeled “flare” sequence (~10 bases long) that is hybridized to the particle. In this state, the fluorophore label is close to the particle surface, and its fluorescence is predominantly quenched. In the cell, the nanoflare particle encounters and binds to its complementary mRNA target, which is longer than the short flare sequence. This action displaces the flare from the particle surface and causes an increase in signal (Figure 12A). One interesting aspect of the nanoflare architecture is that the short flare sequence makes the strands at the surface more rigid and pushes the mRNA complement away from the NP surface, which results in an activated binding site for the mRNA target.<sup>150</sup> Indeed, the kinetics of target binding to sequences with nanoflares is 5 times faster than to single-stranded SNA–Au NP conjugates of the same sequence but without flares.<sup>150</sup> Cells treated with flares of the sequence complementary to the target exhibit much higher fluorescence than cells incubated with noncomplementary flares (Figure 12B). Moreover, the background fluorescence of nanoflares is substantially lower

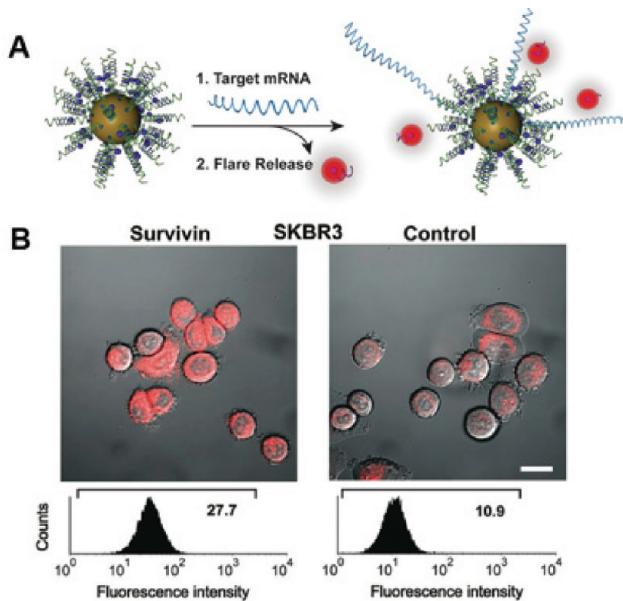


**Figure 12.** (A) Schematic of nanoflares. Short fluorophore-labeled “flare” sequences are hybridized to SNAs targeted for a disease gene of interest. Upon flare particle binding to its mRNA complement, the short flare sequence is displaced and released from the gold core. The flare is no longer quenched when it is released, and therefore a large signal increase is observed. (B) SKBR3 cells, which overexpress survivin, are treated with nanoflare probes targeted for survivin (left) and a nonsense control (right). Samples treated with the survivin flare show 3 times the fluorescence of cells treated with the control flare particles. Reproduced with permission from ref 11. Copyright 2007 American Chemical Society.

than that of molecular beacons, which is due to increased nuclease resistance of the SNA-based nanoflare structure; indeed, intracellular degradation of the probe beacon leads to significant background fluorescence. Finally, nanoflares allow for simultaneous gene knockdown and mRNA detection from a single conjugate.<sup>51</sup>

One can build upon the nanoflare concept by introducing moieties that rely on other mechanisms of signal transduction or by targeting small molecules instead of mRNA. Nuclear magnetic resonance (NMR) probes have been synthesized by replacing the fluorophore moiety on the flare strand with a sequence of five NMR-active fluorine-19 (<sup>19</sup>F)-modified 5-fluorouracil nucleobases. <sup>19</sup>F is a good choice for this system because fluorine is not very abundant in biological systems. In addition, <sup>19</sup>F is nearly NMR invisible when on the particle but shows a strong signal when released.<sup>151</sup> These probes have a high signal-to-noise ratio (~27) and show a marked increase in signal when they bind their targets. Probes can also be synthesized that target small molecules instead of DNA or RNA sequences. For example, aptamers<sup>152</sup> are oligonucleotides selected for binding affinity and specificity toward a target molecule, and they can be used as the recognition element on the particles to create “aptamer nanoflares” (ANFs).<sup>125</sup> In a proof-of-concept system, ANFs were targeted to adenosine triphosphate (ATP) because of its importance in cellular metabolism regulation and biochemical pathways. Duplexes formed from the known ATP aptamer sequence and short complementary flare sequences were conjugated to Au NPs to form ATP-ANFs. In the presence of ATP, the ATP aptamer changes its conformation to bind ATP, which displaces the flare

sequence and results in a large fluorescence increase. Significantly, ATP-ANFs can be used to quantify intracellular amounts of ATP in live cells. In principle, the nanoflare design can be tailored for many intracellular molecular targets and with many possible labeling and readout strategies. In principle, these include techniques like computed tomography and positron emission tomography. These strategies may lead to a broader impact on medicine and cancer treatments in general, including treatments specific for gene expression profiles or live small-molecule tracking within organs.

## 11. CONCLUSIONS AND OUTLOOK

SNAs have emerged as a fundamental new class of nucleic acid constructs with a set of properties distinct from linear forms of nucleic acids of the same sequence. These properties have led to powerful new concepts in materials synthesis and colloidal crystallization and laid the foundation for important new technologies in the life sciences and medicine. They were initially made to introduce a simple concept for nanoparticle assembly whereby programmable base-pairing interactions could be used to reversibly form macroscopic materials from nanoscale components. However, the discovery that the arrangement of oligonucleotides into highly oriented, densely packed spherical structures results in entities capable of interacting with biological materials in unique ways provided venues to use them in molecular diagnostics, gene regulation, and medicine. These constructs do not simply provide different ways of accomplishing what can be done with molecular systems but rather superior approaches. This is apparent in *in vitro* molecular diagnostics where SNA cooperative binding and subsequent melting lead to higher selectivity in assays based upon SNA probes, in gene regulation, where the densely packed and oriented nucleic acids in SNAs can support the binding of scavenger proteins, which trigger endocytosis, and in the case of nanoflares, where the ability of SNAs to freely enter cells combined with their ability to resist nuclease degradation gives rise to a powerful new class of live single-cell assays.

Significantly, the understandings garnered from the studies of SNAs as diagnostic and gene-regulating constructs brought the initial study of DNA-mediated assembly full circle through the realization of some of the key insights required for nanoparticle crystallization, which has emerged as a rich field of study in the past few years. Many researchers around the globe have made significant contributions to the field of SNAs as it continues to expand across diverse scientific and technological disciplines. However, there is still much to be learned about the fundamental properties of SNAs, their scope of utility, and the diversity of possible conjugate materials. We still do not understand their modes of intracellular trafficking at the molecular level, why they can penetrate tissues and organs much more effectively than analogous molecular systems, and how they move from cell to cell within living systems. The bulk of the technologies based upon them have focused on the life sciences, but there are significant opportunities in the areas of electronics, catalysis, and energy harvesting, storage, and conversion. The realization of such opportunities will rely on our ability to synthesize broader classes of conjugate materials. Indeed, although the majority of the work carried out thus far has focused on SNA–Au NP conjugates, we and others have shown that SNAs can be prepared from magnetic,<sup>43</sup> insulator,<sup>58</sup> semiconductor,<sup>44</sup> and metallic materials,<sup>1</sup> and even pure DNA cores prepared by DNA origami techniques.<sup>156</sup>

Anisotropic SNA nanostructures are just beginning to be explored, and their use as near-infrared plasmonic heating materials and surface-enhanced Raman spectroscopy labels may prove useful not only in the development of new biodiagnostic and imaging tools but also in the realization of plasmonic energy conversion materials. Because of their tailororable binding strengths, anisotropic 3D nucleic acids may find use in novel detection assays with higher sensitivities than analogous assays with SNAs. Collectively, these SNA conjugate structures, combined with a fundamental understanding of their properties, will establish a new paradigm in bioprogrammable particle design. Indeed, they should inspire new syntheses of bioconjugated nanomaterials based on the functions one can realize from the cooperative behavior of ligand shells combined with the exquisitely tailororable properties of nanomaterial cores.

## ■ ASSOCIATED CONTENT

### Supporting Information

Complete ref 144. This material is available free of charge via the Internet at <http://pubs.acs.org>.

## ■ AUTHOR INFORMATION

### Corresponding Author

chadnano@northwestern.edu

## ■ ACKNOWLEDGMENTS

C.A.M. acknowledges the DOE Office (Award No. DE-SC0000989) for support through the Northwestern Non-equilibrium Energy Research Center (NERC). He also acknowledges the NSF-NSEC and the AFOSR for grant support, and is grateful for an NSSEF Fellowship from the DoD. E.A. acknowledges the NDSEG for a Graduate Research Fellowship and Northwestern University for a Ryan Fellowship.

## ■ REFERENCES

- Mirkin, C. A.; Letsinger, R. L.; Mucic, R. C.; Storhoff, J. J. *Nature* **1996**, *382*, 607–609.
- Jain, K. K. *Exp. Rev. Mol. Diagn.* **2003**, *3*, 153–161.
- Farokhzad, O. C.; Langer, R. *Adv. Drug Delivery Rev.* **2006**, *58*, 1456–1459.
- Storhoff, J. J.; Elghanian, R.; Mucic, R. C.; Mirkin, C. A.; Letsinger, R. L. *J. Am. Chem. Soc.* **1998**, *120*, 1959–1964.
- Taton, T. A.; Mirkin, C. A.; Letsinger, R. L. *Science* **2000**, *289*, 1757–1760.
- Rosi, N. L.; Mirkin, C. A. *Chem. Rev.* **2005**, *105*, 1547–1562.
- Weiss, S.; Bruchez, M.; Moronne, M.; Gin, P.; Alivisatos, A. P. *Science* **1998**, *281*, 2013–2016.
- Morrow, D. A.; Wilson, S. R.; Sabatine, M. S.; Braunwald, E.; Sloan, S.; Murphy, S. A. *Am. Heart J.* **2009**, *158*, 386–391.
- Verma, A.; Simard, J. M.; Worrall, J. W.; Rotello, V. M. *J. Am. Chem. Soc.* **2004**, *126*, 13987–91.
- Xu, X. H. N.; Kyriacou, S. V.; Brownlow, W. *J. Biochemistry* **2004**, *43*, 140–147.
- Seferos, D. S.; Giljohann, D. A.; Hill, H. D.; Prigodich, A. E.; Mirkin, C. A. *J. Am. Chem. Soc.* **2007**, *129*, 15477–15479.
- Giljohann, D. A.; Seferos, D. S.; Daniel, W. L.; Massich, M. D.; Patel, P. C.; Mirkin, C. A. *Angew. Chem., Int. Ed.* **2010**, *49*, 3280–3294.
- Sandhu, K. K.; McIntosh, C. M.; Simard, J. M.; Smith, S. W.; Rotello, V. M. *Bioconjugate Chem.* **2002**, *13*, 3–6.
- Lehr, C. M.; Kumar, M. N. V. R.; Sameti, M.; Mohapatra, S. S.; Kong, X.; Lockey, R. F.; Bakowsky, U.; Lindenblatt, G.; Schmidt, H. *J. Nanosci. Nanotechnol.* **2004**, *4*, 876–881.
- Rosi, N. L.; Giljohann, D. A.; Thaxton, C. S.; Lytton-Jean, A. K. R.; Han, M. S.; Mirkin, C. A. *Science* **2006**, *312*, 1027–1030.
- von Maltzahn, G.; Park, J. H.; Lin, K. Y.; Singh, N.; Schwoppe, C.; Mesters, R.; Berdel, W. E.; Ruoslahti, E.; Sailor, M. J.; Bhatia, S. N. *Nat. Mater.* **2011**, *10*, 545–552.
- Giljohann, D. A.; Seferos, D. S.; Prigodich, A. E.; Patel, P. C.; Mirkin, C. A. *J. Am. Chem. Soc.* **2009**, *131*, 2072–2073.
- Davis, M. E.; Chen, Z.; Shin, D. M. *Nat. Rev. Drug Discov.* **2008**, *7*, 771–782.
- Dobson, J. *Gene Ther.* **2006**, *13*, 283–287.
- Cutler, J. I.; Zhang, K.; Zheng, D.; Auyeung, E.; Prigodich, A. E.; Mirkin, C. A. *J. Am. Chem. Soc.* **2011**, *133*, 9254–9257.
- Leff, D. V.; Brandt, L.; Heath, J. R. *Langmuir* **1996**, *12*, 4723–4730.
- Kataby, G.; Cojocaru, M.; Prozorov, R.; Gedanken, A. *Langmuir* **1999**, *15*, 1703–1708.
- Johnson, S. R.; Evans, S. D.; Brydson, R. *Langmuir* **1998**, *14*, 6639–6647.
- Zheng, W.; Maye, M. M.; Leibowitz, F. L.; Zhong, C. J. *The Analyst* **1999**, *125*, 17–20.
- Galow, T.; Boal, A.; Rotello, V. *Adv. Mater.* **2000**, *12*, 576–579.
- Dubois, L. H.; Nuzzo, R. G. *Annu. Rev. Phys. Chem.* **1992**, *43*, 437–463.
- Bain, C. D.; Whitesides, G. M. *Angew. Chem., Int. Ed.* **1989**, *28*, 506–512.
- Mucic, R. C.; Herrlein, M. K.; Mirkin, C. A.; Letsinger, R. L. *Chem. Commun.* **1996**, 555–557.
- Alivisatos, A. P.; Johnsson, K. P.; Peng, X. G.; Wilson, T. E.; Loweth, C. J.; Bruchez, M. P.; Schultz, P. G. *Nature* **1996**, *382*, 609–611.
- Sonnichsen, C.; Reinhard, B. M.; Liphardt, J.; Alivisatos, A. P. *Nat. Biotechnol.* **2005**, *23*, 741–745.
- Liu, N.; Hentschel, M.; Weiss, T.; Alivisatos, A. P.; Giessen, H. *Science* **2011**, *332*, 1407–1410.
- Luger, K.; Mader, A. W.; Richmond, R. K.; Sargent, D. F.; Richmond, T. J. *Nature* **1997**, *389*, 251–260.
- Fei, J.; Richard, A. C.; Bronson, J. E.; Gonzalez, R. L. *Nat. Struct. Mol. Biol.* **2011**, *18*, 1043–1051.
- Bansal, M.; Ghosh, A. *Acta Crystallogr. D* **2003**, *59*, 620–626.
- Dean, D. A.; Vaughan, E. E.; DeGiulio, J. V. *Curr. Gene Ther.* **2006**, *6*, 671–681.
- Seeman, N. C. *Nature* **2003**, *421*, 427–431.
- Seeman, N. *Trends Biotechnol.* **1999**, *17*, 437–443.
- Han, D.; Pal, S.; Nangreave, J.; Deng, Z.; Liu, Y.; Yan, H. *Science* **2011**, *332*, 342–346.
- Lytton-Jean, A. K. R.; Mirkin, C. A. *J. Am. Chem. Soc.* **2005**, *127*, 12754–12755.
- Jin, R. C.; Wu, G. S.; Li, Z.; Mirkin, C. A.; Schatz, G. C. *J. Am. Chem. Soc.* **2003**, *125*, 1643–1654.
- Seferos, D. S.; Prigodich, A. E.; Giljohann, D. A.; Patel, P. C.; Mirkin, C. A. *Nano Lett.* **2009**, *9*, 308–311.
- Lee, J. S.; Lytton-Jean, A. K. R.; Hurst, S. J.; Mirkin, C. A. *Nano Lett.* **2007**, *7*, 2112–2115.
- Cutler, J. I.; Zheng, D.; Xu, X. Y.; Giljohann, D. A.; Mirkin, C. A. *Nano Lett.* **2010**, *10*, 1477–1480.
- Mitchell, G. P.; Mirkin, C. A.; Letsinger, R. L. *J. Am. Chem. Soc.* **1999**, *121*, 8122–8123.
- Han, M. Y.; Liu, S. H. *Adv. Funct. Mater.* **2005**, *15*, 961–967.
- Stoeva, S. I.; Huo, F. W.; Lee, J. S.; Mirkin, C. A. *J. Am. Chem. Soc.* **2005**, *127*, 15362–15363.
- Li, Z.; Zhang, Y.; Fullhart, P.; Mirkin, C. A. *Nano Lett.* **2004**, *4*, 1055–1058.
- Liu, H. P.; Zhu, Z.; Kang, H. Z.; Wu, Y. R.; Sefan, K.; Tan, W. H. *Chem.–Eur. J.* **2010**, *16*, 3791–3797.
- Redl, F. X.; Black, C. T.; Papaefthymiou, G. C.; Sandstrom, R. L.; Yin, M.; Zeng, H.; Murray, C. B.; O'Brien, S. P. *J. Am. Chem. Soc.* **2004**, *126*, 14583–14599.
- Keefe, A. D.; Wilson, C. *Curr. Opin. Chem. Biol.* **2006**, *10*, 607–614.
- Prigodich, A. E.; Seferos, D. S.; Massich, M. D.; Giljohann, D. A.; Lane, B. C.; Mirkin, C. A. *ACS Nano* **2009**, *3*, 2147–2152.

- (52) Seferos, D. S.; Giljohann, D. A.; Rosi, N. L.; Mirkin, C. A. *ChemBioChem* **2007**, *8*, 1230–1232.
- (53) Li, Z.; Jin, R. C.; Mirkin, C. A.; Letsinger, R. L. *Nucleic Acids Res.* **2002**, *30*, 1558–1562.
- (54) Sato, K.; Hosokawa, K.; Maeda, M. *J. Am. Chem. Soc.* **2003**, *125*, 8102–8103.
- (55) Frens, G. *Nature Phys. Sci.* **1973**, *241*, 20–22.
- (56) Park, S. Y.; Lytton-Jean, A. K. R.; Lee, B.; Weigand, S.; Schatz, G. C.; Mirkin, C. A. *Nature* **2008**, *451*, 553–556.
- (57) Nykypanchuk, D.; Maye, M. M.; van der Lelie, D.; Gang, O. *Nature* **2008**, *451*, 549–552.
- (58) Xue, C.; Chen, X.; Hurst, S. J.; Mirkin, C. A. *Adv. Mater.* **2007**, *19*, 4071–4072.
- (59) Cao, Y. W.; Jin, R.; Mirkin, C. A. *J. Phys. Chem. B* **2001**, *123*, 7961–7962.
- (60) Yin, Y. D.; Li, Z. Y.; Zhong, Z. Y.; Gates, B.; Xia, Y. N.; Venkateswaran, S. *J. Mater. Chem.* **2002**, *12*, 522–527.
- (61) Medintz, I. L.; Berti, L.; Pons, T.; Grimes, A. F.; English, D. S.; Alessandrini, A.; Facci, P.; Mattoucci, H. *Nano Lett.* **2007**, *7*, 1741–1748.
- (62) Dougan, J. A.; Karlsson, C.; Smith, W. E.; Graham, D. *Nucleic Acids Res.* **2007**, *35*, 3668–3675.
- (63) Letsinger, R. L.; Elghanian, R.; Viswanadham, G.; Mirkin, C. A. *Bioconjugate Chem.* **2000**, *11*, 289–291.
- (64) Hurst, S. J.; Lytton-Jean, A. K. R.; Mirkin, C. A. *Anal. Chem.* **2006**, *78*, 8313–8318.
- (65) McKenzie, F.; Faulds, K.; Graham, D. *Small* **2007**, *3*, 1866–1868.
- (66) Lytton-Jean, A. K. R.; Gibbs-Davis, J. M.; Long, H.; Schatz, G. C.; Mirkin, C. A.; Nguyen, S. T. *Adv. Mater.* **2009**, *21*, 706–707.
- (67) Dhar, S.; Daniel, W. L.; Giljohann, D. A.; Mirkin, C. A.; Lippard, S. *J. Am. Chem. Soc.* **2010**, *132*, 17335–17335.
- (68) Song, Y.; Xu, X. Y.; MacRenaris, K. W.; Zhang, X. Q.; Mirkin, C. A.; Meade, T. J. *Angew. Chem., Int. Ed.* **2009**, *48*, 9143–9147.
- (69) Xu, X. Y.; Daniel, W. L.; Wei, W.; Mirkin, C. A. *Small* **2010**, *6*, 623–626.
- (70) Nam, J. M.; Thaxton, C. S.; Mirkin, C. A. *Science* **2003**, *301*, 1884–1886.
- (71) Kim, D.; Daniel, W. L.; Mirkin, C. A. *Anal. Chem.* **2009**, *81*, 9183–9187.
- (72) Zhang, X.-Q.; Xu, X.; Lam, R.; Giljohann, D.; Ho, D.; Mirkin, C. A. *ACS Nano* **2011**, *5*, 6962–6970.
- (73) Elghanian, R.; Storhoff, J. J.; Mucic, R. C.; Letsinger, R. L.; Mirkin, C. A. *Science* **1997**, *277*, 1078–1081.
- (74) Giljohann, D. A.; Seferos, D. S.; Patel, P. C.; Millstone, J. E.; Rosi, N. L.; Mirkin, C. A. *Nano Lett.* **2007**, *7*, 3818–3821.
- (75) Hill, H. D.; Millstone, J. E.; Banholzer, M. J.; Mirkin, C. A. *ACS Nano* **2009**, *3*, 418–424.
- (76) Storhoff, J. J.; Elghanian, R.; Mirkin, C. A.; Letsinger, R. L. *Langmuir* **2002**, *18*, 6666–6670.
- (77) Taton, T. A.; Mucic, R. C.; Mirkin, C. A.; Letsinger, R. L. *J. Am. Chem. Soc.* **2000**, *122*, 6305–6306.
- (78) Wang, H.; Xu, W.; Zhang, H.; Li, D.; Yang, Z.; Xie, X.; Li, T.; Liu, X. *Small* **2011**, *7*, 1987–1992.
- (79) Zwanikken, J. W.; Guo, P. J.; Mirkin, C. A.; de la Cruz, M. O. *J. Phys. Chem. C* **2011**, *115*, 16368–16373.
- (80) Gibbs-Davis, J. M.; Nguyen, S. T.; Schatz, G. C. *J. Am. Chem. Soc.* **2007**, *129*, 15535–15540.
- (81) Park, S. Y.; Gibbs-Davis, J. M.; Nguyen, S. B. T.; Schatz, G. C. *J. Phys. Chem. B* **2007**, *111*, 8785–8791.
- (82) Eryazici, I.; Prytkova, T. R.; Schatz, G. C.; Nguyen, S. T. *J. Am. Chem. Soc.* **2010**, *132*, 17068–17070.
- (83) Stepp, B. R.; Gibbs-Davis, J. M.; Koh, D. L. F.; Nguyen, S. T. *J. Am. Chem. Soc.* **2008**, *130*, 9628–9629.
- (84) Millstone, J. E.; Georganopoulos, D. G.; Xu, X. Y.; Wei, W.; Li, S. Y.; Mirkin, C. A. *Small* **2008**, *4*, 2176–2180.
- (85) Jones, M. R.; Macfarlane, R. J.; Lee, B.; Zhang, J.; Young, K. L.; Senesi, A. J.; Mirkin, C. A. *Nat. Mater.* **2010**, *9*, 913–917.
- (86) Hurst, S. J.; Hill, H. D.; Mirkin, C. A. *J. Am. Chem. Soc.* **2008**, *130*, 12192–12200.
- (87) Wu, Z. S.; Guo, M. M.; Shen, G. L.; Yu, R. Q. *Anal. Bioanal. Chem.* **2007**, *387*, 2623–2626.
- (88) Hurst, S. J.; Hill, H. D.; Macfarlane, R. J.; Wu, J.; Dravid, V. P.; Mirkin, C. A. *Small* **2009**, *5*, 2156–2161.
- (89) Park, S. J.; Lazarides, A. A.; Storhoff, J. J.; Pesce, L.; Mirkin, C. A. *J. Phys. Chem. B* **2004**, *108*, 12375–12380.
- (90) Huo, F. W.; Lytton-Jean, A. K. R.; Mirkin, C. A. *Adv. Mater.* **2006**, *18*, 2304–2305.
- (91) Xu, X. Y.; Rosi, N. L.; Wang, Y. H.; Huo, F. W.; Mirkin, C. A. *J. Am. Chem. Soc.* **2006**, *128*, 9286–9287.
- (92) Maye, M. M.; Nykypanchuk, D.; Cuisinier, M.; van der Lelie, D.; Gang, O. *Nat. Mater.* **2009**, *8*, 388–391.
- (93) Park, S. Y.; Lytton-Jean, A. K. R.; Lee, B.; Weigand, S.; Schatz, G. C.; Mirkin, C. A. *Nature* **2008**, *451*, 553–556.
- (94) Nykypanchuk, D.; Maye, M. M.; Lelie, D. v. d.; Gang, O. *Nature* **2008**, *451*, 549–552.
- (95) Macfarlane, R. J.; Lee, B.; Jones, M. R.; Harris, N.; Schatz, G. C.; Mirkin, C. A. *Science* **2011**, *334*, 204–208.
- (96) Macfarlane, R. J.; Jones, M. R.; Senesi, A. J.; Young, K. L.; Lee, B.; Wu, J.; Mirkin, C. A. *Angew. Chem., Int. Ed.* **2010**, *49*, 4589–4592.
- (97) Xiong, H.; Lelie, D. v. d.; Gang, O. *Phys. Rev. Lett.* **2009**, *102*, 1–4.
- (98) Hill, H. D.; Macfarlane, R. J.; Senesi, A. J.; Lee, B.; Park, S. Y.; Mirkin, C. A. *Nano Lett.* **2008**, *8*, 2341–2344.
- (99) Sun, D.; Gang, O. *J. Am. Chem. Soc.* **2011**, *133*, 5252–5254.
- (100) Pauling, L. *J. Am. Chem. Soc.* **1929**, *51*, 1010–1026.
- (101) Xia, Y. N.; Xiong, Y. J.; Lim, B.; Skrabalak, S. E. *Angew. Chem., Int. Ed.* **2009**, *48*, 60–103.
- (102) Jones, M. R.; Osberg, K. D.; Macfarlane, R. J.; Langille, M. R.; Mirkin, C. A. *Chem. Rev.* **2011**, *111*, 3736–3827.
- (103) Odom, T. W.; Nehl, C. L. *ACS Nano* **2008**, *2*, 612–616.
- (104) Kelly, K. L.; Coronado, E.; Zhao, L. L.; Schatz, G. C. *J. Phys. Chem. B* **2003**, *107*, 668–677.
- (105) Dick, K. A.; Deppert, K.; Larsson, M. W.; Martensson, T.; Seifert, W.; Wallenberg, L. R.; Samuelson, L. *Nat. Mater.* **2004**, *3*, 380–384.
- (106) Hyeon, T.; Park, S. J.; Kim, S.; Lee, S.; Khim, Z. G.; Char, K. *J. Am. Chem. Soc.* **2000**, *122*, 8581–8582.
- (107) Nikoobakht, B.; El-Sayed, M. A. *Chem. Mater.* **2003**, *15*, 1957–1962.
- (108) Millstone, J. E.; Park, S.; Shuford, K. L.; Qin, L. D.; Schatz, G. C.; Mirkin, C. A. *J. Am. Chem. Soc.* **2005**, *127*, 5312–5313.
- (109) Smith, D. K.; Korgel, B. A. *Langmuir* **2008**, *24*, 644–649.
- (110) Poon, L.; Zandberg, W.; Hsiao, D.; Erno, Z.; Sen, D.; Gates, B. D.; Branda, N. R. *ACS Nano* **2010**, *4*, 6395–6403.
- (111) Jones, M. R.; Millstone, J. E.; Giljohann, D. A.; Seferos, D. S.; Young, K. L.; Mirkin, C. A. *ChemPhysChem* **2009**, *10*, 1461–1465.
- (112) Wijaya, A.; Schaffer, S. B.; Pallares, I. G.; Hamad-Schifferli, K. *ACS Nano* **2009**, *3*, 80–86.
- (113) Huschka, R.; Zuloaga, J.; Knight, M. W.; Brown, L. V.; Nordlander, P.; Halas, N. J. *J. Am. Chem. Soc.* **2011**, *133*, 12247–12255.
- (114) Lee, S. E.; Liu, G. L.; Kim, F.; Lee, L. P. *Nano Lett.* **2009**, *9*, 562–570.
- (115) Jones, M. R.; Macfarlane, R. J.; Prigodich, A. E.; Patel, P. C.; Mirkin, C. A. *J. Am. Chem. Soc.* **2011**, *133*, 18865–18869.
- (116) Han, M. S.; Lytton-Jean, A. K. R.; Oh, B. K.; Heo, J.; Mirkin, C. A. *Angew. Chem., Int. Ed.* **2006**, *45*, 1807–1810.
- (117) Liu, C. W.; Hsieh, Y. T.; Huang, C. C.; Lin, Z. H.; Chang, H. T. *Chem. Commun.* **2008**, 2242–2244.
- (118) Lander, E. S.; Altshuler, D.; Pollara, V. J.; Cowles, C. R.; Van Etten, W. J.; Baldwin, J.; Linton, L. *Nature* **2000**, *407*, 513–516.
- (119) Zheng, G. F.; Daniel, W. L.; Mirkin, C. A. *J. Am. Chem. Soc.* **2008**, *130*, 9644–9645.
- (120) Liu, J. W.; Lu, Y. *Angew. Chem., Int. Ed.* **2006**, *45*, 90–94.
- (121) Xu, X.; Han, M. S.; Mirkin, C. A. *Angew. Chem., Int. Ed.* **2007**, *46*, 3468–3470.

- (122) Han, M. S.; Lytton-Jean, A. K. R.; Oh, B. K.; Heo, J.; Mirkin, C. A. *Angew. Chem., Int. Ed.* **2006**, *45*, 1807–1810.
- (123) Lee, J. S.; Han, M. S.; Mirkin, C. A. *Angew. Chem., Int. Ed.* **2007**, *46*, 4093–4096.
- (124) Liu, J.; Lu, Y. *J. Am. Chem. Soc.* **2003**, *125*, 6642–6643.
- (125) Lu, Y.; Liu, J. W. *J. Am. Chem. Soc.* **2004**, *126*, 12298–12305.
- (126) Wang, Z. D.; Lee, J. H.; Lu, Y. *Adv. Mater.* **2008**, *20*, 3263–3267.
- (127) Perez, J. M.; O'Loughlin, T.; Simeone, F. J.; Weissleder, R.; Josephson, L. *J. Am. Chem. Soc.* **2002**, *124*, 2856–2857.
- (128) Graham, D.; Thompson, D. G.; Smith, W. E.; Faulds, K. *Nat. Nanotechnol.* **2008**, *3*, 548–551.
- (129) Nam, J.-M.; Thaxton, C. S.; Mirkin, C. A. *Science* **2003**, *301*, 1884–1886.
- (130) Nam, J. M.; Stoeva, S. I.; Mirkin, C. A. *J. Am. Chem. Soc.* **2004**, *126*, 5932–5933.
- (131) Fire, A.; Xu, S. Q.; Montgomery, M. K.; Kostas, S. A.; Driver, S. E.; Mello, C. C. *Nature* **1998**, *391*, 806–811.
- (132) Pardridge, W. M.; Zhang, Y.; Schlachetzki, F. *Mol. Ther.* **2003**, *7*, 11–18.
- (133) Pardridge, W. M.; Zhang, Y.; Zhu, C. N. *Mol. Ther.* **2002**, *6*, 67–72.
- (134) Herr, A. E.; Tia, S. Q.; He, M.; Kim, D. *Anal. Chem.* **2011**, *83*, 3581–3588.
- (135) Mintzer, M. A.; Simanek, E. E. *Chem. Rev.* **2009**, *109*, 259–302.
- (136) Kim, D.; Halpern, A. R.; Chen, Y. L.; Corn, R. M. *Anal. Chem.* **2011**, *83*, 2801–2806.
- (137) Young, L. S.; Searle, P. F.; Onion, D.; Mautner, V. J. *Pathol. Biochem.* **2006**, *208*, 299–318.
- (138) Shenoy, D. B.; Amiji, M. M. *CSH Protoc.* **2007**, No. pdb.top9.
- (139) Xia, F.; Zuo, X. L.; Yang, R. Q.; Xiao, Y.; Kang, D.; Vallee-Belisle, A.; Gong, X.; Yuen, J. D.; Hsu, B. B. Y.; Heeger, A. J.; Plaxco, K. W. *Proc. Natl. Acad. Sci. U. S. A.* **2010**, *107*, 10837–10841.
- (140) Liu, J. W.; Lu, Y. *Chem. Mater.* **2004**, *16*, 3231–3238.
- (141) Massich, M. D.; Giljohann, D. A.; Seferos, D. S.; Ludlow, L. E.; Horvath, C. M.; Mirkin, C. A. *Mol. Pharmaceutics* **2009**, *6*, 1934–1940.
- (142) Han, M. S.; Ryoo, S. M.; Kim, S.; Jang, H. H.; Kim, J. H.; Yeom, J. H.; Eom, M. S.; Bae, J.; Lee, K. *Biochem. Biophys. Res. Commun.* **2010**, *398*, 542–546.
- (143) Chithrani, B. D.; Ghazani, A. A.; Chan, W. C. W. *Nano Lett.* **2006**, *6*, 662–668.
- (144) Matsumoto, A. *Proc. Natl. Acad. Sci. U.S.A.* **1990**, *87*, 9133–9137.
- (145) Greaves, D. R.; Gordon, S. J. *Lipid Res.* **2005**, *46*, 11–20.
- (146) Bijsterbosch, M. K.; Manoharan, M.; Rump, E. T.; DeVreue, R. L. A.; vanVeghel, R.; Tivel, K. L.; Biessen, E. A. L.; Bennett, C. F.; Cook, P. D.; vanBerkel, T. J. C. *Nucleic Acids Res.* **1997**, *25*, 3290–3296.
- (147) Schatz, G. C.; Lee, O. S. *J. Phys. Chem. C* **2009**, *113*, 2316–2321.
- (148) Prigodich, A. E.; Alhasan, A. H.; Mirkin, C. A. *J. Am. Chem. Soc.* **2011**, *133*, 2120–2123.
- (149) De Jong, W. H.; Hagens, W. I.; Krystek, P.; Burger, M. C.; Sips, A. J. A. M.; Geertsma, R. E. *Biomaterials* **2008**, *29*, 1912–1919.
- (150) Prigodich, A. E.; Lee, O. S.; Daniel, W. L.; Seferos, D. S.; Schatz, G. C.; Mirkin, C. A. *J. Am. Chem. Soc.* **2010**, *132*, 10638–10641.
- (151) Kieger, A.; Wiester, M. J.; Procissi, D.; Parrish, T. B.; Mirkin, C. A.; Thaxton, C. S. *Small* **2011**, *7*, 1977–1981.
- (152) Ellington, A. D.; Szostak, J. W. *Nature* **1990**, *346*, 818–822.
- (153) Auyeung, E.; Cutler, J. I.; Macfarlane, R. J.; Jones, M. R.; Wu, J.; Liu, G.; Zhang, K.; Osberg, K. D.; Mirkin, C. A. *Nature Nanotech* **2012**, *7*, 24–28.
- (154) Georganopoulou, D. G.; Chang, L.; Nam, J.-M.; Thaxton, C. S.; Mufson, E. J.; Klein, W. L.; Mirkin, C. A. *Proc. Natl. Acad. Sci. U.S.A.* **2005**, *102*, 2273–2276.
- (155) Thaxton, C. S.; Elghanian, R.; Thomas, A. D.; Stoeva, S. I.; Lee, J.-S.; Smith, N. D.; Schaeffer, A. J.; Klocker, H.; Horninger, W.;
- Bartsch, G.; Mirkin, C. A. *Proc. Natl. Acad. Sci. U.S.A.* **2009**, *106*, 18437–18442.
- (156) Walsh, S. A.; Yin, H.; Erben, C. M.; Wood, M. J. A.; Tuberfield, A. J. *ACS Nano* **2011**, *5*, 5427–5432.